PHYSICAL REVIEW D **80,** 085025 (2009)

Supersymmetric QCD effects on neutralino dark matter annihilation beyond scalar or gaugino mass unification

Björn Herrmann

Institut für Theoretische Physik und Astrophysik, Universität Würzburg, Am Hubland, D-97074 Würzburg, Germany

Michael Klasen and Karol Kovařík*

Laboratoire de Physique Subatomique et de Cosmologie, Université Joseph Fourier/CNRS-IN2P3/INPG, 53 Avenue des Martyrs, F-38026 Grenoble, France

(Received 30 June 2009; revised manuscript received 25 August 2009; published 28 October 2009)

We describe in detail our calculation of the full supersymmetric QCD corrections to neutralino annihilation into heavy quarks and extend our numerical analysis of the resulting dark matter relic density to scenarios without scalar or gaugino mass unification. In these scenarios, the final state is often composed of top quarks and the annihilation proceeds through Z^0-boson or scalar top-quark exchanges. The impact of the corrections is again shown to be sizable, so that they must be taken into account systematically in global analyses of the supersymmetry parameter space.

DOI: 10.1103/PhysRevD.80.085025 PACS numbers: 12.38.Bx, 12.60.Jv, 95.30.Cq, 95.35.+d

I. INTRODUCTION

The search for physics beyond the standard model (SM) is no longer restricted to colliders only. In fact, the most compelling evidence for new physics comes today from cosmological observations such as the mission of the Wilkinson Microwave Anisotropy Probe (WMAP), which have determined the matter and energy decomposition of our Universe with unprecedented precision. These observations indicate the existence of cold dark matter (CDM) in the Universe, which cannot be accounted for by the SM and likely consists of weakly interacting massive particles (WIMPs) with nonrelativistic velocities. A combination of the five-year measurement of the cosmic microwave background by the WMAP mission with supernova and baryonic acoustic oscillation data yields the narrow 2σ-interval for the relic density of dark matter [1]

$$0.1097 < \Omega_{\mathrm{CDM}} h^2 < 0.1165, \tag{1}$$

where h denotes the present Hubble expansion rate H_0 in units of 100 $\mathrm{km\,s^{-1}\,Mpc^{-1}}$.

The measured relic density of dark matter can be used to constrain extensions of the standard model, which provide a viable WIMP candidate. In the minimal supersymmetric standard model (MSSM) with R-parity conservation, this could be the lightest supersymmetric particle (LSP) $\tilde{\chi}$, if it is neutral and a color singlet. One can then calculate its relic density, compare it with the experimental limits in Eq. (1), and identify the favored regions of the MSSM parameter space. The relic density

$$\Omega_{\tilde{\chi}} h^2 = \frac{n_0 m_{\tilde{\chi}}}{\rho_c} \tag{2}$$

is proportional to the present number density n_0 and the mass $m_{\tilde{\chi}}$ of the LSP. $\rho_c = 3H_0^2/(8\pi G_{\mathrm{N}})$ is the critical density of our Universe, and G_{N} is the gravitational constant. The present number density n_0 is obtained by solving the Boltzmann equation describing the time evolution of the number density

$$\frac{dn_{\tilde{\chi}}}{dt} = -3Hn_{\tilde{\chi}} - \langle \sigma_{\mathrm{ann}} v \rangle (n_{\tilde{\chi}}^2 - n_{\mathrm{eq}}^2). \tag{3}$$

The first term on the right-hand side corresponds to a dilution due to the expansion of the Universe, and the second term corresponds to a decrease due to annihilations and coannihilations of the relic particle into SM particles [2]. Here, H denotes the time-dependent Hubble expansion parameter, and n_{eq} the density of the relic particle in thermal equilibrium. Details of the dark matter interactions enter the Boltzmann equation through the thermally averaged cross section $\langle \sigma_{\mathrm{ann}} v \rangle$. The cross section takes into account the thermal velocity distribution of the relic particle and is calculated for a given temperature T by

$$\langle \sigma_{\mathrm{ann}} v \rangle = \frac{4}{m_{\tilde{\chi}}^4 T K_2^2(\frac{m_{\tilde{\chi}}}{T})} \int dp_{\mathrm{cm}} p_{\mathrm{cm}}^3 \sqrt{s} K_1\left(\frac{\sqrt{s}}{T}\right) \sigma_{\mathrm{ann}}(s), \tag{4}$$

where K_1 and K_2 are the modified Bessel functions of the first and second kind, respectively. The center-of-momentum energy $\sqrt{s}$ is related to the particle mass $m_{\tilde{\chi}}$ and the relative momentum p_{cm} of the annihilating pair through $s = 4(m_{\tilde{\chi}}^2 + p_{\mathrm{cm}}^2)$ [2].

In order to keep up with current and future experimental improvements, one has to understand and reduce the different uncertainties involved in the analysis, both for the prediction of the dark matter relic density and the extraction of new mass parameters from cosmological data. These uncertainties include, e.g., a modification of the Hubble expansion rate due to quintessence or an effective

*kovarik@lpsc.in2p3.fr

dark energy density [3], differences in the new physical particle masses obtained with different spectrum codes [4], or a lack of precision in the annihilation cross section of dark matter particles [5]. In this paper, we focus on the impact of next-to-leading order QCD and supersymmetric (SUSY)-QCD corrections on the latter, but other possible uncertainties will also be briefly discussed.

In many scenarios of the MSSM, the lightest neutralino is the LSP and therefore a suitable dark matter candidate. The thermally averaged cross section is then obtained by computing all relevant neutralino annihilation cross sections into SM particles. Most prominent are the processes with two-particle final states such as a fermion-antifermion pair or a combination of gauge ($W^{\pm}$, Z^0) and Higgs bosons (h^0, H^0, A^0, $H^{\pm}$) [6,7]. In this paper, we focus on the annihilation into a massive quark-antiquark pair, since the leading order cross section with a fermion-antifermion final state is proportional to the mass of the fermion, which disfavors the light quarks. Moreover, the annihilation into heavy quarks is important in the regions of parameter space allowed by Eq. (1). We now present the full details of our calculation and investigate scenarios with dominant top-quark final-state contributions, extending our analysis of Refs. [8,9] beyond minimal supergravity (mSUGRA) models. In mSUGRA models, one is constrained by having only five universal high-scale parameters [m_0, $m_{1/2}$, A_0, $\tan\beta$, and $\mathrm{sgn}(\mu)$], and in regions of parameter space, where quark final states are important, the cross section is dominated by an exchange of Higgs bosons. Here, we relax the unification of either the scalar masses or the gaugino masses, one at a time. This allows for scenarios different from mSUGRA, where the annihilation cross section is not necessarily dominated by Higgs-boson exchanges. Apart from a Higgs-boson dominated scenario, we thus analyze scenarios where Z^0-boson exchanges in the s-channel or squark exchanges in the t- and u-channels play an important role. The full QCD and SUSY-QCD corrections in these scenarios turn out to be significant, and we have therefore included them into the public code `micrOMEGAs` [10].

This paper is organized as follows: In Sec. II and Appendices A and B, we give all necessary details of the calculation related to the virtual loop corrections, the renormalization procedure, and the calculation of real gluon emission, in particular, the subtraction of the induced soft and collinear singularities. We then continue in Sec. III with a discussion of the MSSM models beyond scalar or gaugino mass unification. In Sec. IV, we analyze the impact of the radiative corrections on the relic density in these models. Finally, our results are summarized in Sec. V.

II. CALCULATION DETAILS

The annihilation of neutralinos into quarks proceeds at tree-level through an exchange of a Z^0-boson and Higgs bosons in the s-channel and through the exchanges of scalar quarks in the t- and u-channels (see Fig. 1). By definition, a WIMP can only have electroweak interactions, and in order to reach a sufficient annihilation rate to explain the dark matter relic density, the cross section has to be enhanced, e.g., by a resonance. One often finds that there is one contribution which dominates the whole cross section. This allows us, by choosing different scenarios, to study contributions from various channels. Moreover, it allows us also to isolate effects of radiative corrections coming from different sources.

We have computed the full QCD and SUSY-QCD corrections to neutralino annihilation into quarks. The next-to-leading order cross section contains virtual contributions stemming from loop diagrams and real contributions, which are due to the radiation of an additional gluon. Symbolically, the next-to-leading order (NLO) cross section can be written as

$$\sigma^{\mathrm{NLO}} = \int_{2\to 2} d\sigma^{\mathrm{V}} + \int_{2\to 3} d\sigma^{\mathrm{R}}, \tag{5}$$

where $\sigma^{\mathrm{V,R}}$ denote the virtual and real emission parts integrated over the two- and three-particle phase space, respectively. The cross section σ^{V}, which includes the tree-level and the one-loop virtual corrections, is given by

$$\sigma^{\mathrm{V}}_{\mathrm{ann}}(s) = \int \frac{1}{16\pi^2}\,\frac{1}{2\kappa(s, m_{\tilde{\chi}}^2, m_{\tilde{\chi}}^2)}\,\frac{\kappa(s, m_q^2, m_q^2)}{2s} \times [|\mathcal{M}_{\mathrm{tree}}|^2 + 2\Re(\mathcal{M}_{1\text{-loop}}\mathcal{M}^*_{\mathrm{tree}})]d\Omega, \tag{6}$$

where $\kappa(x, y, z) = \sqrt{(x - y - z)^2 - 4yz}$. For our notation and conventions, we refer the reader to Appendix A. There are two types of contributions to the one-loop amplitude $\mathcal{M}_{1\text{-loop}}$, those coming from the loop diagrams and those coming from the counterterms. The loop diagrams, depicted in Fig. 2, contain ultraviolet (UV) and infrared (IR) divergent loop integrals. We regulate both types of divergences dimensionally ($d = 4 - 2\epsilon$) and evaluate the loop integrals in the dimensional reduction scheme ($\overline{\mathrm{DR}}$).

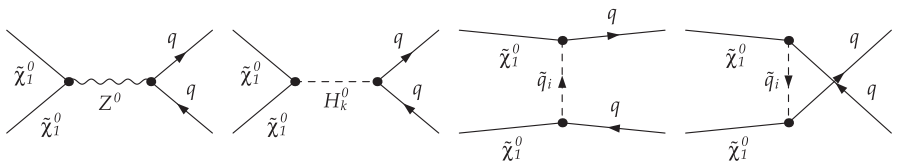

FIG. 1. Tree-level Feynman diagrams for the annihilation of a neutralino pair into a quark-antiquark pair through the exchange of a Z^0-boson, a neutral Higgs-boson $H_k^0 = (h^0, H^0, A^0)$, or a squark $\tilde{q}_i$ ($i = 1, 2$).

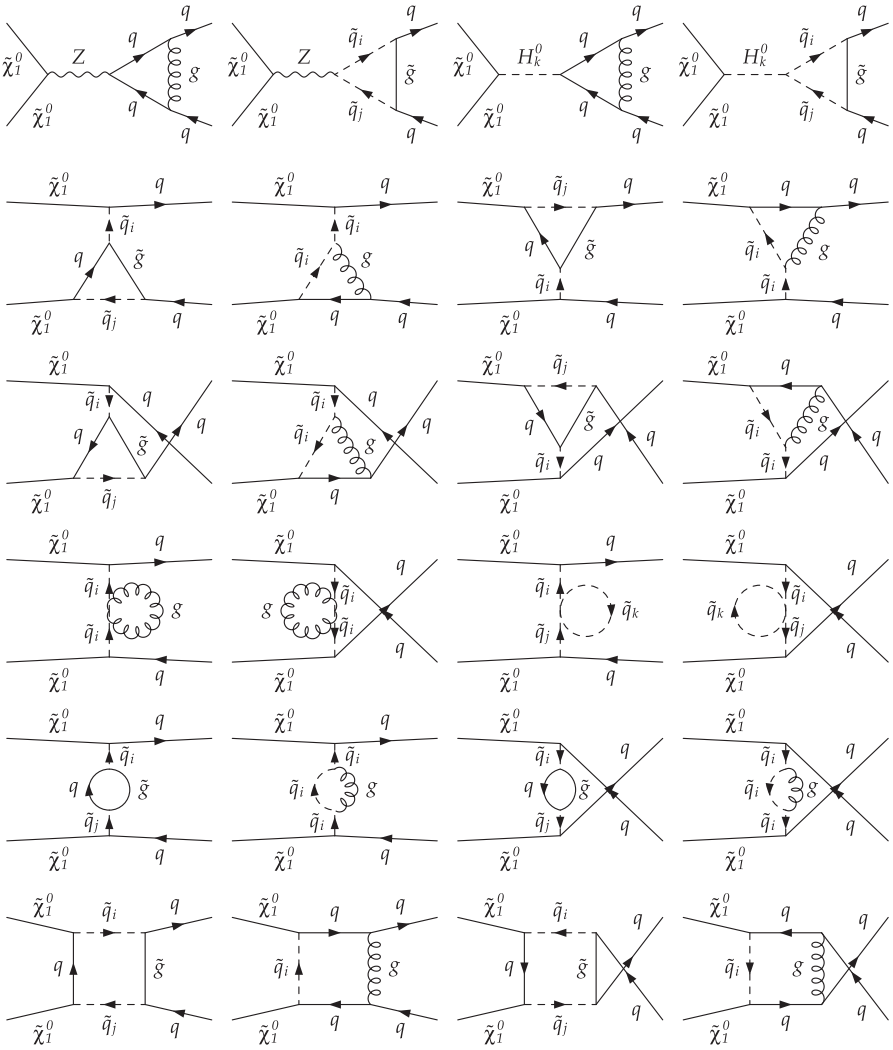

FIG. 2. SUSY-QCD loop diagrams contributing to the annihilation of neutralinos into quarks.

The full analytic results for the loop diagrams are given in Appendix B.

The UV divergences are compensated by counterterms (see Fig. 3) related to quarks and their scalar superpartners, the squarks. All counterterm vertices with quark or squark legs contain wave-function renormalization factors δZ_L, δZ_R and δZ_{ij}, that follow from replacing the (s)quark fields by

$$\begin{pmatrix} q_L \\ q_R \end{pmatrix} \to \begin{pmatrix} 1+\frac{1}{2}\delta Z_L & 0 \\ 0 & 1+\frac{1}{2}\delta Z_R \end{pmatrix} \begin{pmatrix} q_L \\ q_R \end{pmatrix}, \qquad \tilde{q}_i \to \left(\delta_{ij} + \frac{1}{2}\delta Z_{ij}\right)\tilde{q}_j. \tag{7}$$

Although in principle only the wave-function renormalization constants of the external quarks have to be included, we also include the squark renormalization constants, as they allow us to perform simpler UV-convergence checks. In the full calculation, the squark wave-function renormalization constants cancel out. The wave-function renormalization constants are determined by requiring the residues of the propagators to remain at unity even at one-loop order. This condition gives

$$\delta Z_L = \Re\Big[-\Pi_L(m_q^2) - m_q^2(\dot{\Pi}_L(m_q^2) + \dot{\Pi}_R(m_q^2)) + \frac{1}{2m_q}(\Pi_{SL}(m_q^2) - \Pi_{SR}(m_q^2)) - m_q(\dot{\Pi}_{SL}(m_q^2) + \dot{\Pi}_{SR}(m_q^2))\Big], \tag{8}$$

$$\delta Z_R = \delta Z_L(L \leftrightarrow R), \tag{9}$$

$$\delta Z_{ii} = -\Re[\dot{\Pi}_{ii}^{\tilde{q}}(m_{\tilde{q}_i}^2)], \qquad \delta Z_{ij} = \frac{2\Re[\Pi_{ij}^{\tilde{q}}(m_{\tilde{q}_j}^2)]}{m_{\tilde{q}_i}^2 - m_{\tilde{q}_j}^2} \quad \text{for } i \neq j, \tag{10}$$

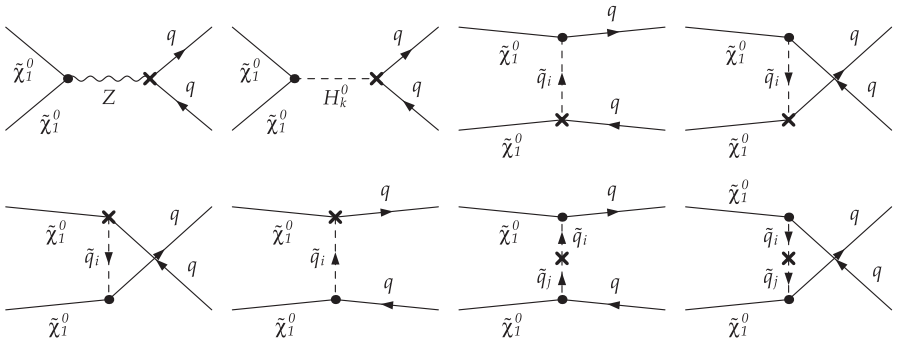

FIG. 3. SUSY-QCD counterterm diagrams contributing to the annihilation of neutralinos into quarks.

where $\Pi_{L,R}(k^2)$ and $\Pi_{SL,SR}(k^2)$ stand for the vector and the scalar parts of the two-point Green's function as defined in Ref. [11] and $\dot{\Pi}(m^2) = [\frac{\partial}{\partial k^2}\Pi(k^2)]_{k^2=m^2}$. After performing the wave-function renormalization, the remaining divergences are canceled by renormalizing the coupling constants. In our case, the coupling counterterms that receive contributions proportional to the strong coupling constant α_s are the quark Yukawa couplings through the masses of the quarks, the squarks masses and the squark mixing angle $\theta_{\tilde{q}}$. A very important contribution, in particular, in scenarios with a dominant Higgs-boson exchange, comes from renormalizing the Yukawa couplings of the quarks [9]. In our calculation, we use the $\overline{\text{DR}}$ Yukawa couplings for both the top and the bottom quarks. As the quark masses that serve as inputs are defined in different schemes, we take two distinct approaches for top and bottom quarks. For top quarks, the input is the on-shell mass $m_t = 172.4$ GeV measured at the Tevatron [12], and the $\overline{\text{DR}}$-mass of the top quark (and hence the $\overline{\text{DR}}$ Yukawa coupling) is obtained by subtracting the finite on-shell counterterm

$$\delta m_q = \frac{1}{2}\Re[m_q(\Pi_L(m_q) + \Pi_R(m_q)) + \Pi_{SL}(m_q) + \Pi_{SR}(m_q)]. \tag{11}$$

On the other hand, the input mass $m_b(m_b)$ for bottom quarks is extracted in the $\overline{\text{MS}}$ renormalization scheme from the standard model analysis of Υ sum rules [13]. In order to obtain the appropriate bottom Yukawa coupling in the $\overline{\text{DR}}$ renormalization scheme within the MSSM, we first use the standard model next-to-next-to-leading order (NNLO) renormalization group evolution to obtain the mass of the bottom quark at the scale $Q = 2m_{\tilde{\chi}}$ [14]. Still in the SM, we then convert $m_b^{\overline{\text{MS}}}(Q)$ to $m_b^{\overline{\text{DR}}}(Q)$ [14], and finally we apply the threshold corrections including also contributions from SUSY particles in the loop. For the last step, we take into account the fact that the sbottom-gluino and stop-chargino one-loop contributions are considerably enhanced for large $\tan\beta$ or large A_b and can be resummed to all orders in perturbation theory [15,16]. Denoting the resummable part by Δ_b and the finite one-loop remainder by Δm_b, the bottom-quark mass is then given by

$$m_b^{\overline{\text{DR}},\text{MSSM}}(Q) = \frac{m_b^{\overline{\text{DR}},\text{SM}}(Q)}{1+\Delta_b} - \Delta m_b. \tag{12}$$

In the squark sector, we pick five independent quantities, $m_{\tilde{t}_1}$, $m_{\tilde{t}_2}$, $m_{\tilde{b}_1}$, $\theta_{\tilde{t}}$, and $\theta_{\tilde{b}}$, in order to respect the SU(2) symmetry. We renormalize the masses of three squarks in the on-shell scheme, which leads to the counterterm

$$\delta m_{\tilde{q}_i}^2 = \Re[\Pi_{ii}^{\tilde{q}}(m_{\tilde{q}_i}^2)]. \tag{13}$$

The remaining mass of the heavier scalar bottom quark $m_{\tilde{b}_2}$ is treated as dependent,

$$\begin{aligned}\delta m_{\tilde{b}_2}^2 = \frac{1}{\sin^2\theta_{\tilde{b}}}[&\delta m_{\tilde{t}_1}^2\cos^2\theta_{\tilde{t}} + \delta m_{\tilde{t}_2}^2\sin^2\theta_{\tilde{t}} - \delta m_{\tilde{b}_1}^2\cos^2\theta_{\tilde{b}} \\ &+ (m_{\tilde{t}_2}^2 - m_{\tilde{t}_1}^2)\sin 2\theta_{\tilde{t}}\delta\theta_{\tilde{t}} \\ &- (m_{\tilde{b}_2}^2 - m_{\tilde{b}_1}^2)\sin 2\theta_{\tilde{b}}\delta\theta_{\tilde{b}}].\end{aligned} \tag{14}$$

The squark mixing angle is renormalized in the $\overline{\text{DR}}$ scheme and so the corresponding counterterms of the squark mixing matrices $R_{ij}^{\tilde{q}}$ contain only the divergent parts. The counterterms can be determined as

$$\delta R_{ij}^{\tilde{q}} = \sum_{k=1}^{2}\frac{1}{4}(\delta Z_{ik}^{\text{div}} - \delta Z_{ki}^{\text{div}})R_{kj}^{\tilde{q}}, \tag{15}$$

using only the divergent parts of the wave-function renormalization constants. This is equivalent to fixing the mixing angle as

$$\begin{aligned}\delta\theta_{\tilde{q}} &= \frac{1}{4}(\delta Z_{12}^{\text{div}} - \delta Z_{21}^{\text{div}}) \\ &= \frac{1}{2(m_{\tilde{q}_1}^2 - m_{\tilde{q}_2}^2)}\Re[\Pi_{12}^{\tilde{q}\text{div}}(m_{\tilde{q}_2}^2) + \Pi_{21}^{\tilde{q}\text{div}}(m_{\tilde{q}_1}^2)].\end{aligned} \tag{16}$$

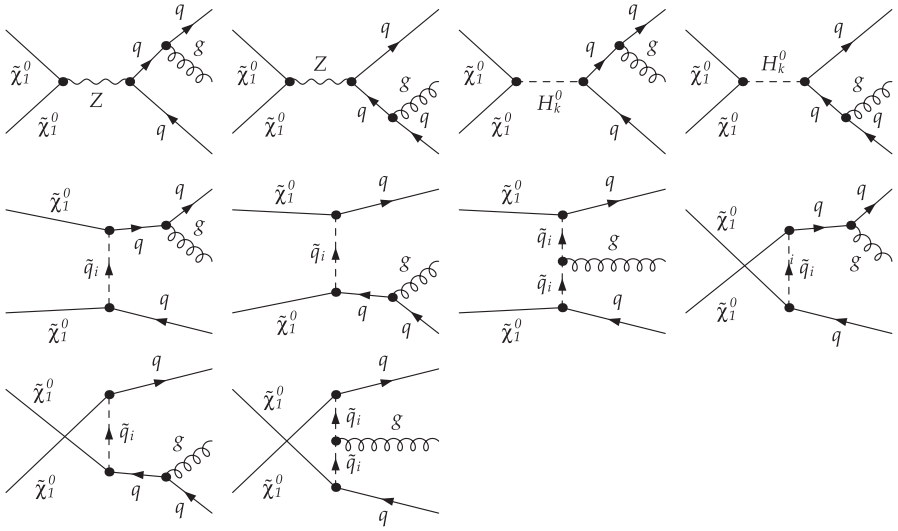

FIG. 4. Bremsstrahlung diagrams contributing to the annihilation of neutralinos into quarks.

After renormalization, the virtual cross section σ^{V} still contains IR divergences, that come from an exchange of a gluon in the loops. In order to compensate them, one has to include the real cross section σ^{R} coming from diagrams with an additional gluon in the final state (see Fig. 4). The symbolic formula of Eq. (5) cannot be directly applied, since the divergences appear as $1/\epsilon$ and $1/\epsilon^2$ poles in the number of dimensions in the one-loop amplitude and as a divergent matrix element in certain regions of the $2 \to 3$ parameter space. A convenient way to combine these two cross sections and to cancel the divergences is the dipole subtraction method [17]. Using this method, we can write the total next-to-leading order cross section σ^{NLO} as

$$\sigma^{\mathrm{NLO}} = \int_{2\to 2}\left[d\sigma^{\mathrm{V}} + \int_1 d\sigma^{\mathrm{A}}\right]_{\epsilon=0} + \int_{2\to 3}[(d\sigma^{\mathrm{R}})_{\epsilon=0} - (d\sigma^{\mathrm{A}})_{\epsilon=0}], \quad (17)$$

where we introduced an auxiliary cross section σ^{A}. The auxiliary cross section does not contribute to the total cross section and serves only as a tool to cancel the IR divergences. It has the same divergence structure as the real cross section and at the same time its structure allows for a partial integration of the gluon phase space, so that it can also be added to the virtual cross section, canceling the divergences in each part. The $2 \to 3$ matrix element leading to the auxiliary cross section for the real part is constructed from two dipole contributions $\mathcal{D}_{31,2}$ and $\mathcal{D}_{32,1}$ as

$$|\mathcal{M}^{2\to 3}_{\mathrm{aux}}|^2 = \mathcal{D}_{31,2}(k_1, k_2, k_3) + \mathcal{D}_{32,1}(k_1, k_2, k_3), \quad (18)$$

where the k_i are the four-momenta of the final-state quarks and of the gluon. The dipole contributions $\mathcal{D}_{31,2}$ and $\mathcal{D}_{32,1}$ are related by a simple interchange $k_1 \leftrightarrow k_2$ with $\mathcal{D}_{31,2}$ given by

$$\begin{aligned}\mathcal{D}_{31,2}(k_1, k_2, k_3) &= C_F \frac{8\pi\alpha_s}{s}|\mathcal{M}_{\mathrm{tree}}|^2 \\ &\times \frac{1}{1-x_2}\left\{\frac{2(1-2\mu_q^2)}{2-x_1-x_2} - \sqrt{\frac{1-4\mu_q^2}{x_2^2-4\mu_q^2}}\frac{x_2-2\mu_q^2}{1-2\mu_q^2}\right. \\ &\times \left.\left[2 + \frac{x_1-1}{x_2-2\mu_q^2} + \frac{2\mu_q^2}{1-x_2}\right]\right\}, \end{aligned} \quad (19)$$

where $x_i = 2k_i.q/q^2$, $\mu_q = m_q/\sqrt{s}$, and $q^2 = (k_1 + k_2 + k_3)^2 = s$ [17]. The leading order matrix element $|\mathcal{M}_{\mathrm{tree}}|^2$ appearing in Eq. (19) is calculated using different kinematics with redefined 4-momenta

$$\begin{aligned} k_1^\mu \to \tilde{k}_{31}^\mu &= \frac{1}{2}q^\mu - \frac{\sqrt{1-4\mu_q^2}}{\sqrt{x_2^2-4\mu_q^2}}\left(k_2^\mu - \frac{1}{2}x_2 q^\mu\right), \\ k_2^\mu \to \tilde{k}_2^\mu &= \frac{1}{2}q^\mu + \frac{\sqrt{1-4\mu_q^2}}{\sqrt{x_2^2-4\mu_q^2}}\left(k_2^\mu - \frac{1}{2}x_2 q^\mu\right). \end{aligned} \quad (20)$$

The auxiliary matrix element that cancels the infrared divergences of the virtual matrix element is

$$\begin{aligned}|\mathcal{M}^{2\to 2}_{\mathrm{aux}}|^2 &= 2C_F\frac{\alpha_s}{2\pi}\frac{(4\pi)^\epsilon}{\Gamma(1-\epsilon)}|\mathcal{M}_{\mathrm{tree}}|^2 \\ &\times \left[\left(\frac{\mu^2}{s_{12}}\right)^\epsilon\left(\mathcal{V}_q(s_{12}, m_q, m_q; \epsilon) - \frac{\pi^2}{3}\right)\right. \\ &+ \left.\frac{1}{C_F}\Gamma_q(m_q;\epsilon) + \frac{3}{2}\ln\frac{\mu^2}{s_{12}} + 5 - \frac{\pi^2}{6}\right], \end{aligned} \quad (21)$$

where $s_{12} = s - 2m_q^2$. The function $\mathcal{V}_q$ is composed of a singular part,

$$\mathcal{V}^{(S)}(s_{12}, m_q, m_q; \epsilon) = \frac{1+\beta^2}{2\beta}\left[\frac{1}{\epsilon}\ln\frac{1-\beta}{1+\beta} - \frac{1}{2}\ln^2\frac{1-\beta}{1+\beta} - \frac{\pi^2}{6} + \ln\frac{1-\beta}{1+\beta}\ln\frac{2}{1+\beta^2}\right] \tag{22}$$

with $\beta = \sqrt{1-4\mu_q^2}$, and a nonsingular part given by

$$\begin{aligned}\mathcal{V}_q^{(NS)}(s_{12}, m_q, m_q) = {} & \frac{3}{2}\ln\frac{1+\beta^2}{2} + \frac{1+\beta^2}{2\beta}\left[2\ln\frac{1-\beta}{1+\beta}\ln\frac{2(1+\beta^2)}{(1+\beta)^2} + 2\,\mathrm{Li}_2\left(\frac{1-\beta}{1+\beta}\right)^2 - 2\,\mathrm{Li}_2\left(\frac{2\beta}{1+\beta}\right) - \frac{\pi^2}{6}\right] \\ & + \ln\left(1-\frac{1}{2}\sqrt{1-\beta^2}\right) - 2\ln(1-\sqrt{1-\beta^2}) - \frac{1-\beta^2}{1+\beta^2}\ln\frac{\sqrt{1-\beta^2}}{2-\sqrt{1-\beta^2}} - \frac{\sqrt{1-\beta^2}}{2-\sqrt{1-\beta^2}} \\ & + 2\frac{1-\beta^2-\sqrt{1-\beta^2}}{1+\beta^2} + \frac{\pi^2}{2}.\end{aligned} \tag{23}$$

The function Γ_q is defined as

$$\Gamma_q(m_q; \epsilon) = C_F\left[\frac{1}{\epsilon} + \frac{1}{2}\ln\frac{m_q^2}{Q^2} - 2\right], \tag{24}$$

where Q is the renormalization scale. Apart from convergence checks of our calculation, we also performed checks of the finite part of the one-loop diagrams against the results obtained by the automatic computer packages `FeynArts` and `FormCalc` [18] and parts of the calculation also against existing results, e.g. in Ref. [19]. The UV and IR divergent parts of our loop integrals were checked and agree with the results given in Ref. [20].

III. SUSY MODELS BEYOND MINIMAL SUPERGRAVITY

In our previous publications, we studied the impact of the SUSY-QCD corrections to neutralino annihilation within minimal supergravity (mSUGRA) models, defined at the grand unification scale $M_{\rm GUT}$ in terms of a universal scalar mass m_0, a universal gaugino mass $m_{1/2}$, a common trilinear coupling A_0, the ratio $\tan\beta$ of the Higgs doublet vacuum expectation values, and the sign of the Higgsino mass parameter μ [8,9]. In mSUGRA models, the lightest neutralino is often a B-ino and annihilates preferably through resonant Higgs-boson exchanges. For example, in the focus-point region at high scalar masses m_0 the cross section is dominated by heavy CP-even Higgs bosons decaying into top quarks. Regions with important bottom-quark final states include those with small gaugino masses $m_{1/2}$, where light CP-even Higgs-boson exchanges dominate, and the A^0-funnel region at high values of $\tan\beta$, where the bottom Yukawa coupling is enhanced and the annihilation proceeds through pseudoscalar Higgs-boson exchanges. At large $\tan\beta$, the bottom-quark contribution can also become sizable in the focus-point region.

In this work, we study in detail numerically the annihilation of neutralinos into top quark-antiquark pairs through the exchange of Z^0-bosons in the s-channel and of top squarks in the t- and u-channels (see Fig. 1). These channels can be enhanced in models, where some of the unification conditions have been relaxed, which is well motivated theoretically [21–23]. To be concrete, we focus on two sets of models based on the SO(10) grand unified theory (GUT): models with nonuniversal Higgs masses (NUHM), and models without gaugino mass unification. SO(10) theories are particularly promising, as they involve complete **16**-dimensional matter multiplets with a right-handed neutrino and can be embedded in string theories involving larger groups like E_8 or SO(32) [24,25].

A. SUSY models with nonuniversal Higgs masses

In SO(10) SUSY GUTs, the matter superfields of one generation belonging to a **16**-dimensional representation are completely mass degenerate, if the SUSY-breaking masses are acquired above the SO(10)-breaking scale. Flavor-blind mechanisms can furthermore lead to universal masses of all matter scalars. However, if the Higgs doublets H_u and H_d belong to different, e.g., **10**-dimensional, representations, the corresponding SUSY-breaking masses need not be the same, i.e., the Higgs masses need not be universal [26–29]. In the scalar part of the general MSSM Lagrangian,

$$\begin{aligned}\mathcal{L}_{\rm soft} \subset {} & -(\tilde{\bar{u}}\mathbf{a_u}\tilde{Q}H_u - \tilde{\bar{d}}\mathbf{a_d}\tilde{Q}H_d - \tilde{\bar{e}}\mathbf{a_e}\tilde{L}H_d + \text{h.c.}) \\ & - \tilde{Q}^\dagger\mathbf{m_Q^2}\tilde{Q} - \tilde{L}^\dagger\mathbf{m_L^2}\tilde{L} - \tilde{\bar{u}}\mathbf{m_{\bar{u}}^2}\tilde{\bar{u}}^\dagger - \tilde{\bar{d}}\mathbf{m_{\bar{d}}^2}\tilde{\bar{d}}^\dagger \\ & - \tilde{\bar{e}}\mathbf{m_{\bar{e}}^2}\tilde{\bar{e}}^\dagger - m_{H_u}^2 H_u^* H_u - m_{H_d}^2 H_d^* H_d \\ & - (bH_uH_d + \text{h.c.}),\end{aligned} \tag{25}$$

the trilinear scalar couplings $\mathbf{a_i}$ and the SUSY-breaking scalar masses $\mathbf{m_i^2}$ are still unified to A_0 and m_0 at the GUT scale, but the SUSY-breaking Higgs-mass parameters m_{H_u} and m_{H_d} are in general different. Models with nonuniversal Higgs masses (NUHM) are therefore defined by the parameters m_0, $m_{1/2}$, A_0, $\tan\beta$, $\mathrm{sgn}(\mu)$, m_{H_u}, and m_{H_d}. Note that in our NUHM models the gaugino masses remain unified to $m_{1/2}$ and electroweak symmetry-breaking (EWSB) is still achieved radiatively, albeit through modified renormalization group equations (RGEs). This leads to a more constrained parameter space in the m_0-$m_{1/2}$ plane as compared to mSUGRA models and to the fact that the minimum conditions of the tree-level Higgs potential

$$\sin\beta = \frac{-2b}{m_{H_u}^2 + m_{H_d}^2 + 2\mu^2}, \tag{26}$$

$$\frac{m_Z^2}{2} = \frac{m_{H_d}^2 - m_{H_u}^2 \tan^2\beta}{\tan^2\beta - 1} - \mu^2, \quad \text{and} \tag{27}$$

$$m_A^2 = m_{H_u}^2 + m_{H_d}^2 + 2\mu^2 \tag{28}$$

allow to replace the parameter b by $\tan\beta$, but not to determine the superpotential parameter μ and the pseudoscalar Higgs-boson mass m_A as functions of m_0 and $m_{1/2}$, as was the case in mSUGRA. It is possible to replace the free parameters m_{H_u} and m_{H_d} by the low-scale parameters μ and m_A. Although we do not make use of this fact in our analysis, it can be useful to consider μ and m_A as free parameters of the model, since they strongly influence the annihilation of neutralinos into quarks and especially the relative weight of each channel. Having m_A as a free parameter means that one can find scenarios, where $m_A^2 \simeq 2m_\chi^2$ and the Higgs-boson exchange dominates the cross section even for smaller values of $\tan\beta$. In mSUGRA, such a scenario was only allowed for values of $\tan\beta \gtrsim 40$. We study this case by choosing the benchmark point I given in Table I. Furthermore, the Higgsino parameter μ influences the Higgsino component of the neutralino. By making it larger, one can enhance the contributions from the Z^0-boson exchange. This can be achieved, as discussed in Ref. [26], by starting with large positive values of m_{H_u} and m_{H_d} at the GUT scale. By virtue of the RGE evolution, $m_{H_u}^2$ is driven to small negative values, while $m_{H_d}^2$ remains positive, which results in a small value of μ as given by Eq. (27). This in turn gives rise to a larger Higgsino fraction of the neutralino and enhances the coupling to Z^0-bosons. Such a scenario corresponds to our point II in Table I. Finally, one can make use of the NUHM RGEs to reduce the values of $\mathbf{m_{\tilde{u}}^2}$ and $\mathbf{m_{\tilde{d}}^2}$. This can be obtained by choosing a large and negative difference $m_{H_u}^2 - m_{H_d}^2$. On top of that, by choosing A_0 to be large and negative, one induces a larger splitting in the third-generation sfermion masses, leading to a scenario (point III in Table I) with a small top squark mass and enhanced t- and u-channel exchanges of top squarks.

B. SUSY models without gaugino mass unification

In the gaugino sector, the situation is somewhat similar to the one in Sec. III A. The breaking of the SO(10) symmetry can proceed via a step involving its SU(5) subgroup. The SU(5) later breaks into the standard model gauge groups SU(3) × SU(2) × U(1) [30] and also determines the properties of the SUSY-breaking mechanism. As pointed out in Refs. [21,22], the breaking of supersymmetry itself is induced by an F-term, while the gaugino masses are generated through a chiral superfield Φ, whose auxiliary component F_Φ acquires a vacuum expectation value. Assuming that the gauginos belong to the adjoint representation **24** of SU(5), the fields Φ and F_Φ can in principle belong to any of the irreducible representations appearing in the symmetric product

$$(\mathbf{24} \otimes \mathbf{24})_{\text{sym}} = \mathbf{1} \oplus \mathbf{24} \oplus \mathbf{75} \oplus \mathbf{200}, \tag{29}$$

or any linear combination thereof. The relations between the gaugino masses M_i at the unification scale are given by the embedding coefficients of the standard model groups in SU(5). Note that these possibilities are all compatible with gauge coupling unification, but only the case where the SUSY-breaking field F_Φ is taken to be a pure singlet (**1**) leads to the gaugino mass universality featured by the mSUGRA model.

The soft SUSY-breaking Lagrangian contains mass terms for the B-ino, W-ino, and gluino,

$$\mathcal{L}_{\text{soft}} \subset -\frac{1}{2}(M_1 \tilde{B}\,\tilde{B} + M_2 \tilde{W}\,\tilde{W} + M_3 \tilde{g}\,\tilde{g} + \text{h.c.}). \tag{30}$$

As argued above, the values of M_1, M_2, and M_3 at the unification scale can be considered as independent parameters. Here, we adopt a commonly used parametrization and introduce the dimensionless parameters

$$x_1 = \frac{M_1}{M_2} \quad \text{and} \quad x_3 = \frac{M_3}{M_2}, \tag{31}$$

which will be used together with the W-ino mass parameter M_2 to describe the gaugino sector. The case $x_1 = x_3 = 1$ reproduces the mSUGRA model with the five parameters m_0, $m_{1/2}$, A_0, $\tan\beta$, and $\text{sgn}(\mu)$ at the unification scale.

Models with nonuniversal gaugino masses have been shown to favor annihilation processes where neutralino

TABLE I. High-scale parameters together with the corresponding neutralino relic density, the contribution from top and bottom quark-antiquark final states to the annihilation cross section obtained with `micrOMEGAs 2.1`, and the mass eigenvalues of the lightest neutralino and the lightest stop for our three selected NUHM scenarios.

	m_0 [GeV]	M_2 [GeV]	A_0 [GeV]	$\tan\beta$	$\text{sgn}(\mu)$	m_{H_u} [GeV]	m_{H_d} [GeV]	$\Omega_{\text{CDM}}h^2$	$t\bar{t}$	$b\bar{b}$	$m_{\tilde{\chi}_1^0}$ (GeV)	$m_{\tilde{t}_1}$ (GeV)
I	500	500	0	10	+	1500	1000	0.118	21.0%	64.0%	207.2	606.4
II	620	580	0	10	+	1020	1020	0.118	51.0%	⋯	223.7	923.8
III	500	500	−1200	10	+	1250	2290	0.113	93.4%	⋯	200.7	259.3

TABLE II. High-scale parameters together with the corresponding neutralino relic density, the contribution from top quark-antiquark final states to the annihilation cross section obtained with micrOMEGAs 2.1, and the mass eigenvalues of the lightest neutralino and the lightest stop for our two selected nonuniversal gaugino mass scenarios.

	m_0 [GeV]	M_2 [GeV]	A_0 [GeV]	$\tan\beta$	sgn(μ)	x_1	x_3	$\Omega_{\rm CDM}h^2$	$t\bar{t}$	$m_{\tilde{\chi}_1^0}$ (GeV)	$m_{\tilde{t}_1}$ (GeV)
IV	320	700	−350	10	+	2/3	1/3	0.114	79.2%	183.4	281.9
V	1500	600	0	10	+	1	4/9	0.104	50.4%	235.6	939.0

annihilation into quarks is mediated by a Z^0-boson exchange and squark exchanges [31–33]. It has also been shown that the key parameter in this context is the gluino mass M_3, since it influences practically all sectors of the low-energy mass spectrum through the renormalization group evolution. A decrease in M_3 induces a decrease of the mass squared $m_{H_u}^2$, which through electroweak symmetry-breaking conditions induces a decrease in the Higgsino mass parameter μ as well. This in turn increases the Higgsino fraction of the neutralino and lowers the pseudoscalar Higgs mass m_A. Moreover, having M_3 independent of the other gaugino mass parameters, it is straightforward to obtain lighter squarks, in particular, the scalar tops. This effect can still be enhanced by decreasing the scalar mass parameter m_0 and by adjusting the trilinear coupling A_0, which influences the squark mass splitting. With scalar tops being light (even becoming eventually the next-to-lightest SUSY particle), the squark exchange dominates the cross section for a B-ino-like neutralino, where a low value of $\tan\beta$ suppresses the Higgs-boson exchange (our point IV in Table II). As the Higgsino fraction of the lightest neutralino increases, the squark exchange is enhanced due to the large Yukawa couplings. In the case of a large Higgsino fraction, also the Z^0-boson exchange becomes important and can take over if the lightest stop is not too close in mass to the lightest neutralino. We analyze the consequences of such a scenario by choosing the point V in Table II.

IV. NUMERICAL RESULTS AND DISCUSSION

Starting from the high-scale parameters, we use the public computer program SPheno 2.2.3 [34] for the numerical evaluation of the renormalization group running in order to obtain the SUSY-breaking parameters at the electroweak scale. The relic density of the neutralino is then evaluated numerically using the public code micrOMEGAs 2.1 [10], where we have included our calculation of the neutralino annihilation cross section into third-generation quarks as discussed in Sec. II. For the standard model input parameters, such as masses and couplings, we refer the reader to Ref. [35], except for the value of the top-quark pole mass, $m_{\rm top} = 172.4$ GeV, which has been taken from Ref. [12].

We have chosen five typical parameter points shown in Tables I and II, that have a dominant neutralino annihilation into top or bottom quarks through Higgs-boson, Z^0-boson or squark exchanges and whose relic density lies reasonably close to the WMAP range of Eq. (1). In all scenarios we only consider relatively low values of $\tan\beta = 10$. In Sec. IV A we analyze the first three parameter points (Table I) where we make use of the possible nonuniversality of the Higgs-boson masses to construct scenarios with cross sections dominated by Higgs-boson, Z^0-boson, and squark exchanges, respectively. In Sec. IV B, we investigate point IV, which corresponds to one of the scenarios without gaugino mass unification discussed in Ref. [31], and the point V, which is motivated by one of the "compressed SUSY" scenarios proposed in Ref. [32]. Our chosen parameter points also satisfy electroweak precision and low-energy constraints such as the measurements of the ρ-parameter, the anomalous magnetic moment of the muon, and the branching ratio of the decay $b \to s\gamma$. Because of the large experimental error on the measurement of $\Delta\rho$ [35], however, only regions featuring very high SUSY masses are excluded at the 2σ-level, so that this constraint does not affect our analysis. We have taken into account the anomalous magnetic moment of the muon by taking the Higgsino mass parameter $\mu > 0$. Negative values are disfavored, since they increase the gap between the recent experimental value and the standard model prediction [36]. The most stringent constraint is given by the inclusive branching ratio of the decay $b \to s\gamma$. Recent experimental measurements from *BABAR*, Belle, and CLEO lead to the combined value [37]

$$\mathrm{BR}\,(b \to s\gamma) = (3.52 \pm 0.25) \times 10^{-4}. \qquad (32)$$

The theoretical prediction of the SUSY contribution is particularly sensitive to the masses of the chargino, the charged Higgs boson, and the lightest scalar quark. We have verified that our parameter points lead to values that lie within 2σ of the above limit using the public codes FeynHiggs 2.6.5 [38] and SusyBSG 1.3 [39]. Note also that the direct mass limits from collider searches are fulfilled [35].

Although the focus of the present paper is the improvement of the annihilation cross section through SUSY-QCD corrections, one should keep in mind that there are also other sources of uncertainties in the calculation of the relic density. From the particle physics side, it is well known that differences in the low-energy mass spectrum may occur when using different spectrum generators. This, in

consequence, may induce a sizable difference in the prediction of the dark matter relic density or other observables [4]. Note that, in this context, also the numerical value of the standard model parameters, in particular, the top-quark mass, can influence the favored regions of parameter space, in particular, in the case of dominant annihilation into top-quark final states. Corrections to the annihilation cross section are also induced by the electroweak interaction [5], but these are generally smaller than the strong corrections and beyond the scope of this work. Concerning cosmology, it has been shown that modifications of the standard cosmological model may also affect the prediction of the dark matter relic density. Including, e.g., an energy content such as quintessence or an effective dark density due to extra dimensions modifies the expansion rate or the entropy density of the early universe (see, e.g., [3]) and thus enters into the calculation of the relic density.

The results for all benchmark points from Tables I and II are shown on Figs. 5–12, where Figs. 5 and 6 correspond to benchmark point I, Figs. 7 and 8 correspond to point II, Figs. 7 and 9 correspond to point III, Figs. 10 and 11 correspond to point IV and Figs. 10 and 12 correspond to point V. In the left panels of Figs. 5, 7, and 10, we show the cross section for the annihilation of a neutralino pair into a bottom and/or top quark-antiquark pair as a function of the center-of-momentum energy p_{cm} calculated at the tree-level with $\overline{\mathrm{DR}}$ Yukawa couplings (solid lines) as well as the leading contributions from the individual annihilation channels (dashed lines) and their interferences (dotted lines). Note that some of the latter have been multiplied by (-1) in order to fit into the logarithmic plot. We also show, in arbitrary units, the thermal velocity distribution function, involved in the calculation of the thermal average evaluated at the freeze-out temperature (shaded areas).

In the right panels of Figs. 5, 7, and 10, we show again the total annihilation cross section into bottom and/or top quark-antiquark pairs at different levels of precision, i.e., at leading order with $\overline{\mathrm{DR}}$ couplings (dash-dotted lines), in the approximation included in the `micrOMEGAs` code (dashed lines), which uses effective couplings to absorb the leading loop effects, and with our full one-loop QCD and SUSY-QCD corrections (solid lines). The shaded area indicates again the thermal velocity distribution of the neutralinos at the freeze-out temperature in arbitrary units.

In order to generalize our results, the remaining Figs. 6, 8, 9, 11, and 12 show scans in various two parameter planes

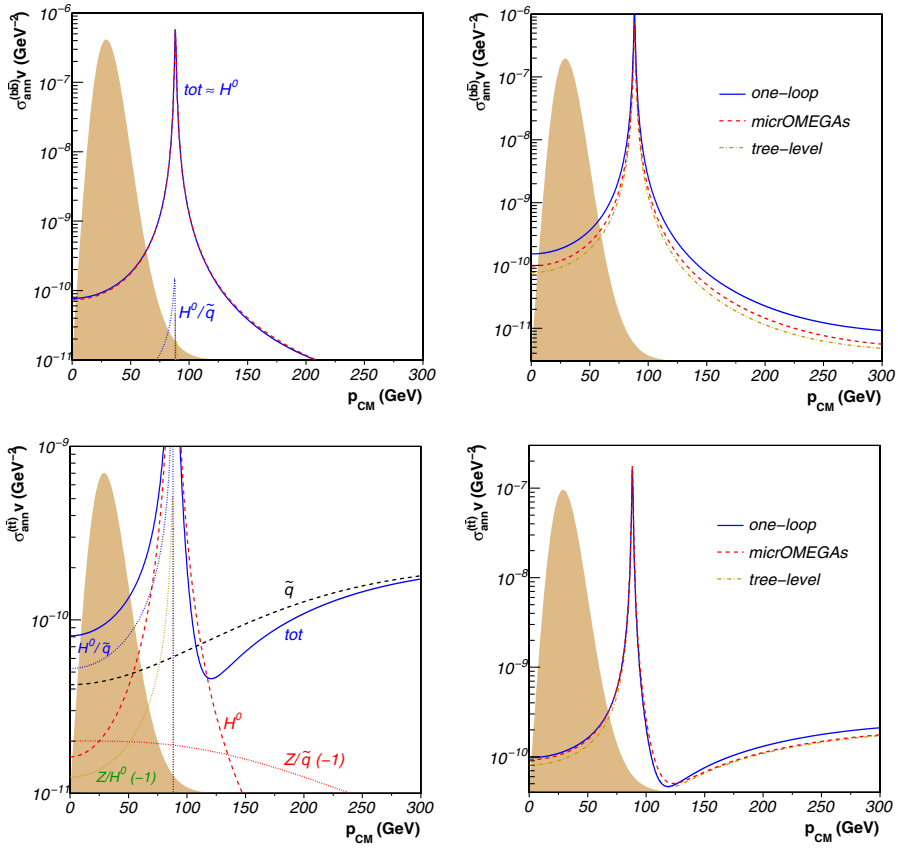

FIG. 5 (color online). The contributions of the different diagrams to the annihilation cross section of a neutralino pair into bottom (above) and top (below) quark-antiquark pairs (left) and the effect of the radiative corrections on the annihilation cross sections (right) as a function of the center-of-momentum energy p_{cm} for our parameter point I. The shaded area indicates the velocity distribution of the neutralino at the freeze-out temperature in arbitrary units.

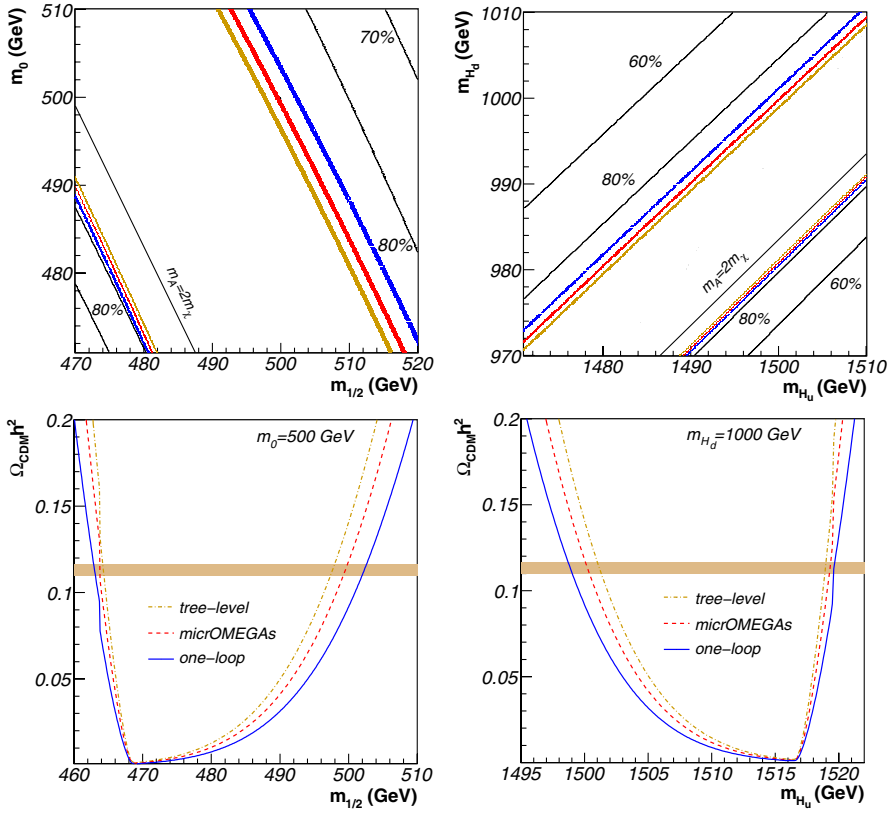

FIG. 6 (color online). Top: Cosmologically favored regions in the m_0-$m_{1/2}$-plane (top left) and m_{H_u}-m_{H_d}-plane (top right) for scans around our parameter point I. We show the regions that satisfy the constraint from Eq. (1) for our tree-level calculation (orange/light grey), the calculation implemented in micrOMEGAs (red/grey), and our calculation including the full SUSY-QCD corrections (blue/dark grey). We also indicate the contributions from quark-antiquark final states to the total annihilation cross section by isolines. Bottom: The prediction of the neutralino relic density $\Omega_{\mathrm{CDM}}h^2$ including the tree-level (orange dash-dotted) cross section, the approximation included in micrOMEGAs (red/grey dashed), and the full one-loop SUSY-QCD corrected cross section (blue/dark grey solid) as a function of the gaugino mass parameter $m_{1/2}$ (left) and as a function of m_{H_u} parameter (right). The shaded area indicates the favored region of Eq. (1).

around our parameter points in Tables I and II and display the contours allowed by WMAP calculated at tree-level (orange/light grey), with the approximation implemented in micrOMEGAs (red/grey), and with our full SUSY-QCD corrections (blue/dark grey). We also show dependence of the relic density on various physical parameters, e.g. the mass of the lightest neutralino.

A. Relic density in models with nonuniversal Higgs masses

We begin our detailed numerical discussion by analyzing a scenario, where the annihilation cross section into quarks is dominated by an exchange of a Higgs boson. This scenario corresponds to our parameter point I from Table I. Here the heavy *CP*-even and the *CP*-odd Higgs-boson resonances coincide with both Higgs-boson masses at 450.3 GeV. Because of the dominance of the Higgs-boson exchange, the neutralino annihilates predominantly into bottom quarks. This is a consequence of the fact that, although the bottom quarks have a much smaller mass compared to the top quarks, their couplings to the Higgs bosons are enhanced by $\tan\beta$ or $\cos\alpha$. As opposed to mSUGRA, the neutralino in this scenario is rather heavy, which allows for an effective annihilation into top quarks as well. In the bottom panels of Fig. 6, a small discontinuity indicates the place, where the top-quark final state starts to contribute. These circumstances result in a mixture of top and bottom-quark final states, which cannot be reached in mSUGRA for such a low value of $\tan\beta$. A few general features can be observed in Figs. 5 and 6. First, on-resonance annihilation of neutralinos would reduce the relic density too much, so that regions allowed by Eq. (1) sit on each side of the resonance peak. In Fig. 5 one can clearly see that the resonance is not aligned with the kinematic region where the biggest contribution to the relic density comes from. The top panels in Fig. 6 display the bands where quark final states dominate the annihilation. In addition, we show a line that corresponds to the position of the Higgs resonance peak. The WMAP allowed regions are situated on each side of the resonance where the width of the these regions reflects the steepness of the peak. The SUSY-QCD corrections to the relic density calculated here

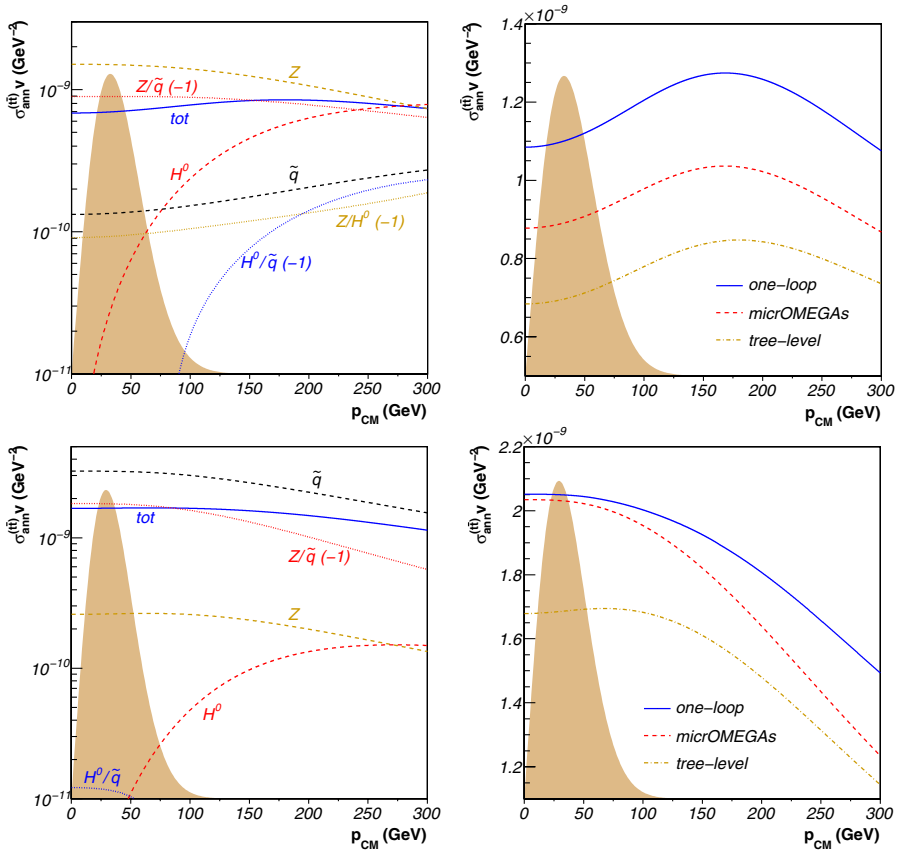

FIG. 7 (color online). The contributions of the different diagrams to the annihilation cross section of a neutralino pair into top quark-antiquark pairs (left) and the effect of the radiative corrections on the annihilation cross section (right) as a function of the center-of-momentum energy p_{cm} for our parameter points II (above) and III (below). The shaded area indicates the velocity distribution of the neutralino at the freeze-out temperature in arbitrary units.

are a combination of corrections to the processes with either bottom or top quarks final states. The corrections to the annihilation into bottom quarks are essentially confined to the Higgs-quark-antiquark vertex. The bulk of the correction comes from the gluon exchange and from the SUSY corrections which become large at large $\tan\beta$ and have to be resummed. As we take a moderate $\tan\beta = 10$ even the nonresummable corrections play a role here. These corrections amount to the difference between our full SUSY-QCD result and the effective coupling approximation implemented in micrOMEGAs in this scenario. The situation with the top quarks is more complicated. As can be seen from Fig. 5, the squark exchanges in the t- and u-channels and their interference with the Higgs-boson exchange become now also sizable, which renders also the corrections to squark-quark-neutralino vertex and to the squark propagator important. Overall for this scenario, the effect of the full SUSY-QCD corrections amounts to a 20% shift in the prediction of the relic density with respect to the calculation implemented in micrOMEGAs, as can be seen in the bottom panels of Fig. 6. In consequence, the cosmologically favored regions of parameter space are shifted away from the position of the Higgs pole in order to compensate the larger annihilation cross section. These shifts amount to up to 5 GeV for the common scalar and gaugino masses and a few GeV for the masses of the Higgs doublets at the unification scale (see Fig. 6). This is about 2 times larger than the experimental precision, and therefore distinct bands appear.

The remaining analyzed scenarios were chosen so as to investigate effects not related to Higgs-boson exchanges. The Higgs-boson masses are very heavy in these scenarios ($m_{H^0}, m_A > 1100$ GeV) and suppress the importance of the Higgs-boson s-channel exchange. The parameter point II in Table I was chosen as described in Sec. III A so that the Z^0-boson exchange is enhanced. The only viable way to do this is to increase the Higgsino fraction of the neutralino, which in turn increases the coupling of neutralinos to the Z^0 boson. Another possibility would be to sit on the Z^0-boson resonance, which would, however, lead to very small neutralino and chargino masses that are already ruled out by the LEP experiments. The parameter point III in Table I was picked to use the Higgs potential high-scale parameters to drive down the squark masses via the renormalization group evolution. On top of that, by choosing $A_0 = -1200$ GeV we induced a large mixing of the third-

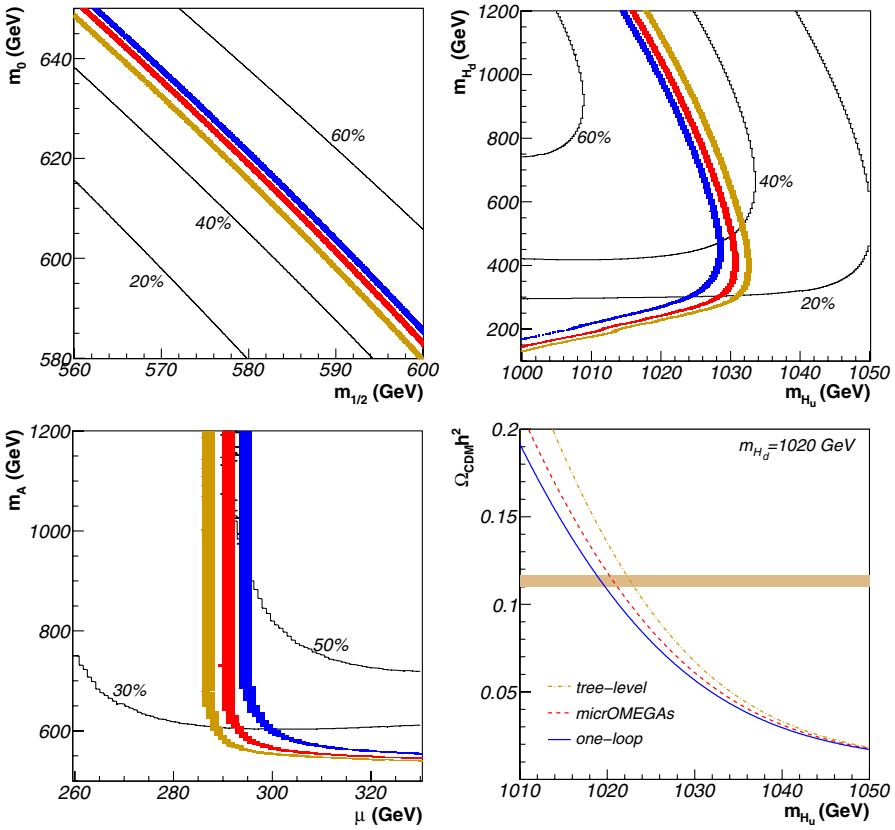

FIG. 8 (color online). Top and bottom left: Scans around our parameter point II in the m_0-$m_{1/2}$-plane, m_{H_u}-m_{H_d}-plane, and m_A-μ-plane. Bottom right: The prediction of the neutralino relic density $\Omega_{\rm CDM}h^2$ as a function of the high-scale Higgs-mass parameter m_{H_u}. The labels are the same as in Fig. 6.

generation squarks. The mixing is biggest for scalar tops increasing the contribution of their exchange. A feature common to both scenarios is a distinct destructive interference between the squark and the Z^0 boson which links these two scenarios (see Fig. 7). This fact makes corrections to both Z^0-boson and squark-exchange important in each of the two scenarios. In the case of the parameter point II, the corrections are about 20% in the cross section as compared to the cross section in `micrOMEGAs`. This is not reflected in all regions of the WMAP allowed regions in Fig. 8, since the contribution of the quark-antiquark final state falls to only 60%–40%, as we lower the Higgsino parameter μ. This decreases the masses of the lightest chargino and of the second-lightest neutralino, which, through their t-channel exchange, increase the annihilation cross sections into W^+W^- and Z^0Z^0 final states. Nevertheless, the full SUSY-QCD corrections shift the contour in the m_A-μ plane by 5 GeV in μ and in all instances shift the contour by more than the current experimental precision. The effect of the corrections to the cross section is not screened by other final states in the case of the scenario with a dominant squark exchange (point III in Table I). The top-quark final state accounts in certain regions for more than 90% of the annihilation cross section, and the mass of the scalar top is not light enough to allow for efficient coannihilations. The hyperbolic shape of the WMAP allowed regions in the m_{H_u}-m_{H_d} plane is governed by the Higgs-mass parameter combination $m^2_{H_u}$-$m^2_{H_d}$. The effect of the corrections on the cross section is about 20% and causes a shift of the preferred value of the pseudoscalar Higgs-boson mass by about 50 GeV.

B. Relic density in models without gaugino mass unification

The relevant masses of our points III and IV featuring very light stops are very similar, as can be seen in Tables I and II. The same holds for the annihilation cross sections. For the benchmark point IV, the exchange of a stop in the t- or u-channel is therefore favored, which is well visible in the top left panel of Fig. 10. The contribution from the Z^0-boson exchange is here 1 order of magnitude lower than the one from squark exchange. Again, an important role is played by the squark Z^0-boson interference effect, which is here even stronger than in the case of point III. The differences are the Higgs-boson masses, which were more than 2000 GeV for point III, but are $m_{H^0,A^0} \simeq$ 622 GeV here (see Fig. 10). The mass difference can be traced back to the mechanism by which we lowered the

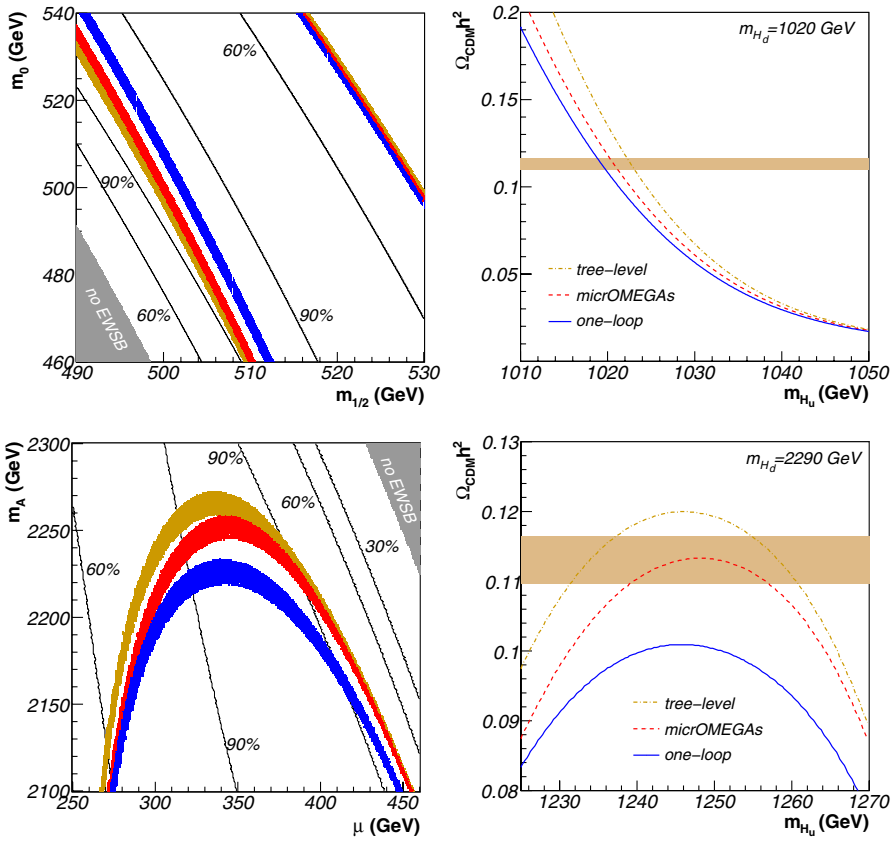

FIG. 9 (color online). Top and bottom left: Scans around our parameter point III in the m_0-$m_{1/2}$-plane, m_{H_u}-m_{H_d}-plane, and m_A-μ-plane. Bottom right: The prediction of the neutralino relic density $\Omega_{\mathrm{CDM}}h^2$ as a function of the high-scale Higgs-mass parameter m_{H_u}. The labels are the same as in Figs. 6 and 8.

squark masses. For point III, we had to induce a big difference between the high-scale Higgs potential parameters, which drove the Higgs-boson masses higher, whereas for point IV we changed freely the gluino mass parameter influencing the RGEs for the squark masses, which has not such a big effect on the masses of the Higgs bosons. Because of the large contribution from the exchange of the light squark, the annihilation into top quarks accounts for up to 80% of the total annihilation cross section (see Fig. 11). The subdominant final states here are again W^+W^- and Z^0Z^0, but also pairs of bottom quarks or leptons. Note that also here the mass difference between the lightest neutralino and the lightest stop is not small enough for efficient coannihilations. One small but important difference is that the destructive interference is stronger for point IV than for point III. This leads to negative correction effects when including the full SUSY-QCD corrections (when compared to the cross section of `micrOMEGAs`). The reason is that for this particular point the corrections to the squark exchange are effectively taken into account by including $\overline{\mathrm{DR}}$ Yukawa couplings and the only difference between our full calculation and the `micrOMEGAs` approximation are the corrections to the interference which push the full result down (as seen in the top right part of Fig. 10). Let us now turn to the impact of the corrections in this "compressed SUSY" scenario. The corresponding favored regions in the m_0-M_2 and the m_0-x_3 planes, the projection on the $m_{\tilde{t}_1}$-$m_{\tilde{\chi}}$ plane as well as the prediction of the neutralino relic density as a function of the gaugino mass parameter M_2 around our parameter point IV are shown in Fig. 11. Again, in the regions where annihilation into a top quark-antiquark pair is kinematically allowed, the effect of the SUSY-QCD corrections is sizable, resulting in an important shift of the favored regions in the parameter space. The preferred region of parameter space is shifted to higher values of the scalar mass parameter m_0 and consequently to higher stop masses $m_{\tilde{t}_1}$. As already discussed above, a heavier stop mass compensates the increasing effect of the additional loop diagrams on the annihilation cross section. In the right bottom panel of Fig. 11 one sees again that the prediction of the relic density is decreased by the order of 15% with respect to the tree-level calculation and by about 10% with respect to the approximation implemented in `micrOMEGAs`.

For our point V with a dominant Z^0-boson exchange, the correction accounts for about 20% of the `micrOMEGAs` cross section. Although `micrOMEGAs` does not include any correction for the exchange of a Z^0-boson, the corresponding curve is approximately 20% over the tree-level

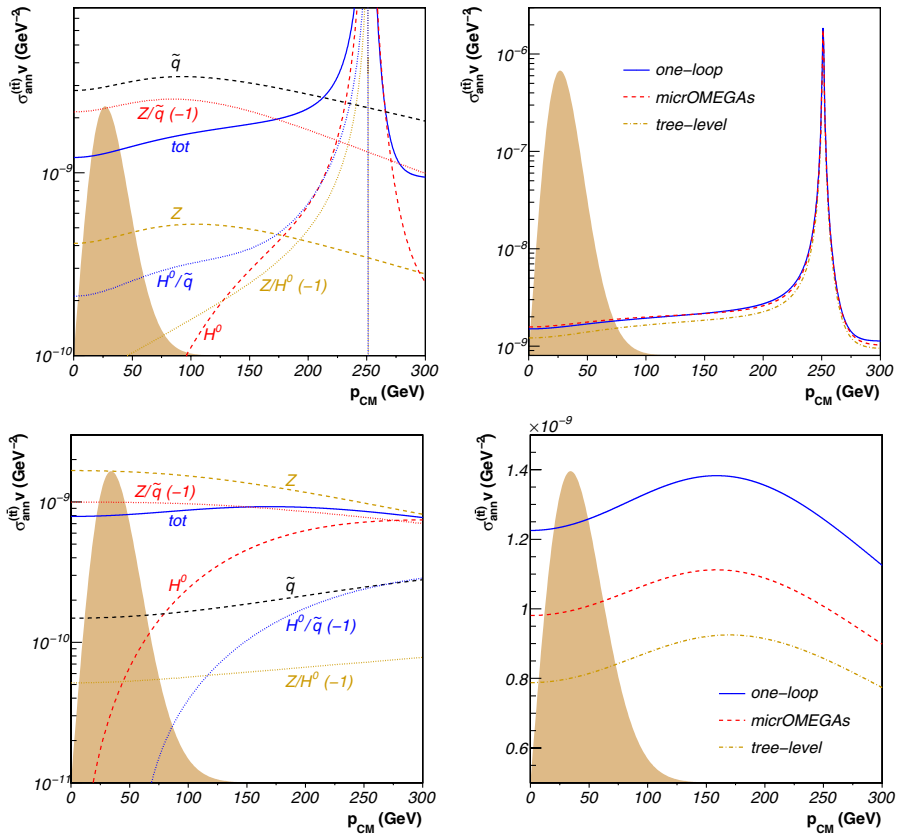

FIG. 10 (color online). The contributions of the different diagrams to the annihilation cross section of a neutralino pair into top quark-antiquark pairs (left) and the effect of the radiative corrections on the annihilation cross section (right) as a function of the center-of-momentum energy $p_{\rm cm}$ for our parameter points IV and V. The shaded area indicates the velocity distribution of the neutralino at the freeze-out temperature in arbitrary units.

prediction, which can be explained by the presence of effective couplings for the subleading squark-exchange. The difference between the approximation included in micrOMEGAs and our full one-loop calculation originates from the supplementary corrections, especially for the exchange of the Z^0-boson, shown in Figs. 2 and 4 and discussed in Sec. II. We study again the influence of our corrections on the regions of parameter space that are favored with respect to the WMAP limits of Eq. (1). The upper left panel of Fig. 12 shows these regions in the m_0-M_2 plane for our scenario V and fixed values of x_1 and x_3 as given in Table II. In the lower left panel, we show the same contours projected on the corresponding plane of the physical neutralino and stop masses $m_{\tilde{\chi}}$ and $m_{\tilde{t}_1}$. In each plot, we also indicate the isocontours corresponding to a contribution from top quark-antiquark final states of 50%, 30%, and 10% to the total neutralino annihilation cross section. The points lying in the grey shaded areas do not allow for physical solutions of the renormalization group equations. The correction to the relic density is reduced from the 20% it was at the cross-section level (as compared with the micrOMEGAs cross section), because the quark-antiquark final state constitutes only about 50% of the annihilation cross section. The remaining contributions include mostly W^+W^- and Z^0Z^0 final states. Nevertheless, as it was also the case for the mSUGRA scenarios analyzed in Ref. [9], the impact of the one-loop SUSY-QCD corrections is larger than the experimental uncertainty. Therefore distinct bands are observed in wide regions of both the m_0-M_2 and in the $m_{\tilde{\chi}}$-$m_{\tilde{t}_1}$ planes. Note that for $M_2 \lesssim 450$ GeV, the annihilation of a neutralino pair into top quarks is kinematically forbidden. The dominating channels for that region are mainly the annihilation into combinations of the gauge bosons and the light Higgs boson. In the m_0-x_3 plane, shown in the right top panel of Fig. 12, the WMAP-favored points are confined to rather narrow bands corresponding to the different levels of included corrections. This underlines that M_3 is one of the key parameters to which phenomenology is very sensitive. It is interesting that for lower values of x_3 their positions are almost independent of m_0, while for higher x_3 the dependence becomes stronger. The shift from the tree-level prediction to our full one-loop result is in the direction of higher gluino masses $M_3 = x_3 M_2$. This is explained by the fact that increasing the gluino mass implies an increase in the squark masses, which in turn implies a decrease of the annihilation cross section. This effect is then combined with the increase of the cross section due to the one-loop

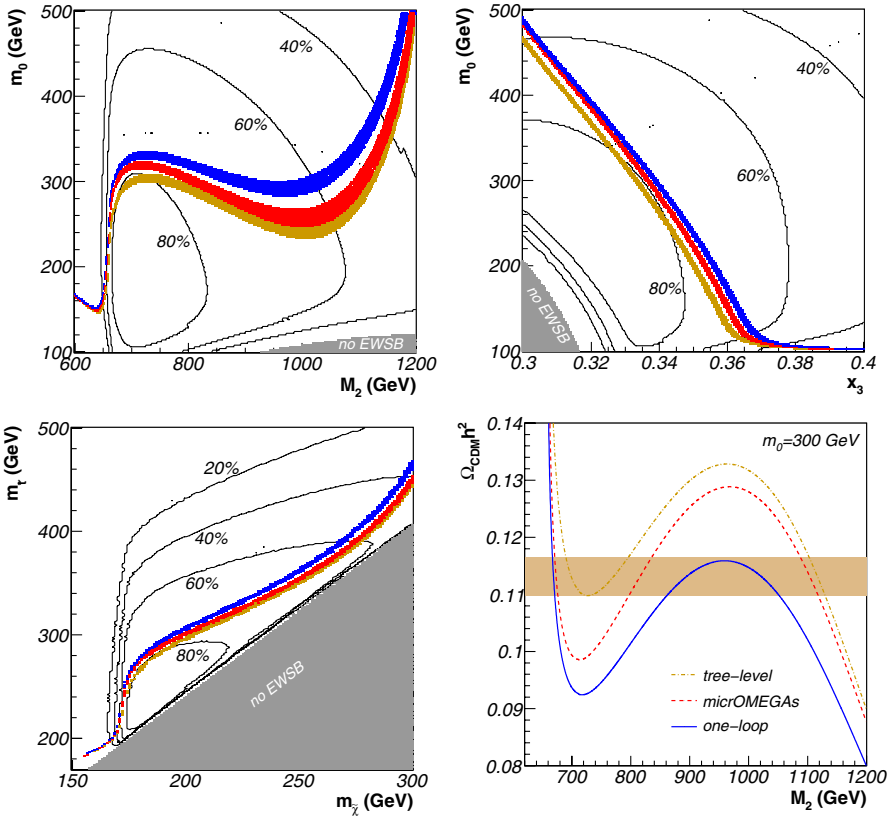

FIG. 11 (color online). Top and bottom left: Cosmologically favored regions in the m_0-M_2-plane (top left), $m_{\tilde{\chi}}$-$m_{\tilde{\tau}}$-plane (bottom left), and m_0-x_3-plane (top right) for scans around our parameter point IV. We show the regions that satisfy the constraint from Eq. (1) for our tree-level calculation (orange/light grey), the calculation implemented in micrOMEGAs (red/grey), and our calculation including the full SUSY-QCD corrections (blue/dark grey). We also indicate the contributions from top-quark final states to the total annihilation cross section by isolines. Excluded regions due to unphysical solutions of the renormalization group equations are shown in gray. Bottom right: The prediction of the neutralino relic density $\Omega_{\mathrm{CDM}}h^2$ including the tree-level (orange dash-dotted) cross section, the approximation included in micrOMEGAs (red/grey dashed), and the full one-loop SUSY-QCD corrected cross section (blue/dark grey solid) as a function of the high-scale gaugino mass parameter M_2 for fixed $m_0 = 300$ GeV. The shaded area indicates the favored region of Eq. (1).

corrections discussed above, so that the relic density remains in the narrow range which is favored by cosmological data. Finally, in the right bottom panel of Fig. 12, we show the prediction for the neutralino relic density $\Omega_{\tilde{\chi}}h^2$ as a function of the lightest stop mass $m_{\tilde{t}_1}$. The neutralino mass has been fixed to the value $m_{\tilde{\chi}} = 235.6$ GeV of our point V. The graph corresponds to a cut through the $m_{\tilde{\chi}}$-$m_{\tilde{t}_1}$ plane shown in the lower left panel of Fig. 12. The favored region of Eq. (1) is indicated by a shaded area. Since the SUSY-QCD corrections increase the annihilation cross section by about 50%, the prediction for the neutralino relic density is reduced by about the same amount.

V. CONCLUSIONS

The theoretical calculation of the dark matter relic density is an interesting tool to obtain rather stringent constraints on the MSSM parameter space, both at the electroweak and at the grand unification scale. Cosmological precision measurements therefore play an important role in the extraction of SUSY mass parameters from experimental data. In times of increasing experimental sensitivity, in particular, for the cosmological parameters such as the relic density of cold dark matter, it is essential to increase the accuracy of the theoretical calculation. Consequently, higher-order corrections to the dark matter annihilation cross section become important, since they enter directly into the calculation of the relic density.

We have presented here the full analytic details of our calculation of the $\mathcal{O}(\alpha_s)$ corrections to the annihilation of a neutralino pair into a massive quark-antiquark pair, i.e., of the one-loop and real gluon emission corrections. Annihilation processes into heavy quarks have been shown to be important in large cosmologically allowed regions of

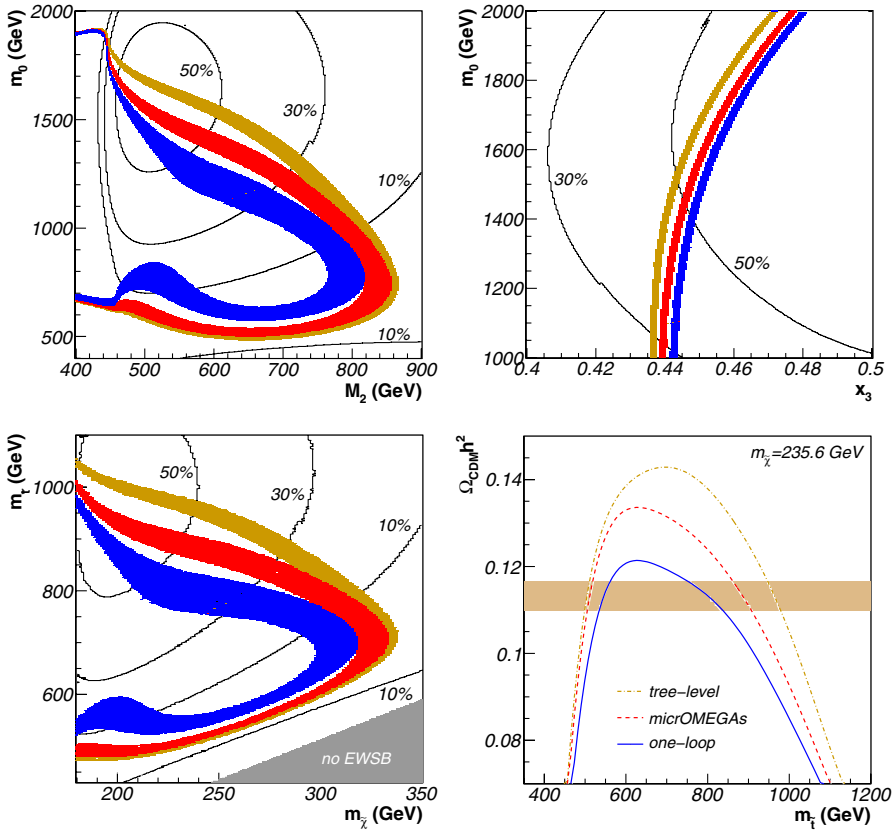

FIG. 12 (color online). Top and bottom left: Scans around our parameter point V in the m_0-M_2-plane (top left), $m_{\tilde{\chi}}$-$m_{\tilde{t}}$-plane (bottom left), and m_0-x_3-plane (top right). Bottom right: The prediction of the neutralino relic density $\Omega_{\mathrm{CDM}}h^2$ as a function of the stop mass $m_{\tilde{t}_1}$ for a fixed neutralino mass $m_{\tilde{\chi}} = 235.6$ GeV. The labels are the same as in Fig. 11.

SUSY GUT models without scalar or gaugino mass unification, and the effects of our SUSY-QCD corrections have been investigated numerically for these two classes of models. We have identified regions of parameter space, which correspond to current cosmological limits on the dark matter relic density and which feature important annihilations of the neutralino pair into a top quark-antiquark pair through the exchange of a Z^0-boson or a scalar quark. Higgs-boson resonances were shown to be suppressed in those regions. For five selected parameter points, the effects of the corrections were shown to be sizable, since they enhanced the annihilation cross section by typically 20 and up to 50% with respect to the tree-level calculation.

As a consequence, the theoretical prediction of the neutralino relic density is also affected by the contributions at the one-loop level. Since the cross section is increased by typically 20 and up to 50%, the relic density is reduced by about the same amount. We have shown that the impact of our corrections is more important than the uncertainty on the observational limits at the 2σ confidence level. It is therefore essential to take these corrections into account when analyzing cosmological data with the goal of extracting SUSY mass parameters, which may be shifted by typically 5 GeV and up to 50 GeV, and of determining the favored regions of the SUSY parameter space.

ACKNOWLEDGMENTS

The authors would like to thank A. Pukhov for his help in implementing the results into the `micrOMEGAs` code and W. Porod for useful discussions. The work of K. K. is supported by the ANR projects ANR-06-JCJC-0038-01 and ToolsDMColl BLAN07-2-194882. The work of B. H. is supported by the DFG project PO 1337/1-1.

APPENDIX A: NOTATION AND COUPLINGS

We follow closely the notation of the couplings defined in Ref. [40] and the conventions used in Refs. [11,19] and begin by listing all necessary couplings of the Z^0-boson. The couplings of fermions to the Z^0-boson in the MSSM are identical to those in the SM, and the Lagrangian is

$$\mathcal{L} = -\frac{g}{c_W} Z^0_\mu \bar{f} \gamma^\mu (C^f_L P_L + C^f_R P_R) f, \qquad \text{(A1)}$$

where g is the weak coupling constant, $C^f_L = I^{3L}_f - e_f s^2_W$, $C^f_R = -e_f s^2_W$, s_W (c_W) is the (co-)sine of the weak mixing

angle θ_W, and I_f^{3L} and e_f are the weak isospin and electric charge of the fermion f. The Lagrangian for the interaction of the Z^0-boson with two neutralinos is given by

$$\mathcal{L} = \frac{g}{2c_W} Z^0_\mu \bar{\tilde{\chi}}^0_i \gamma^\mu (O''^L_{ij} P_L + O''^R_{ij} P_R) \tilde{\chi}^0_j, \tag{A2}$$

where

$$O''^L_{ij} = -\frac{1}{2} Z_{i3} Z_{j3} + \frac{1}{2} Z_{i4} Z_{j4} = -O''^R_{ij} \tag{A3}$$

depend bilinearly on the neutralino mixing matrix Z. The Lagrangian of the Z^0-boson coupling to two sfermions

$$\mathcal{L} = -i \frac{g}{c_W} Z^0_\mu \tilde{f}^*_i z^{\tilde{f}}_{ij} \overleftrightarrow{\partial^\mu} \tilde{f}_j \tag{A4}$$

is proportional to

$$z^{\tilde{f}}_{ij} = C^f_L R^{\tilde{f}}_{i1} R^{\tilde{f}}_{j1} + C^f_R R^{\tilde{f}}_{i2} R^{\tilde{f}}_{j2}, \tag{A5}$$

which depends bilinearly on the sfermion mixing matrix

$$R = (R_{iL}, R_{iR}) = \begin{pmatrix} \cos\theta_{\tilde{f}} & \sin\theta_{\tilde{f}} \\ -\sin\theta_{\tilde{f}} & \cos\theta_{\tilde{f}} \end{pmatrix}. \tag{A6}$$

We continue with the couplings containing neutral Higgs bosons, where we use the notation $H^0_k = \{h^0, H^0, A^0, G^0\}$. $t/\tilde{t}$ stands for an up-type (s)fermion and $b/\tilde{b}$ for a down-type one. For the neutral Higgs-boson-fermion-fermion couplings, the interaction Lagrangian reads

$$\mathcal{L} = \sum_{k=1}^{2} s^f_k H^0_k \bar{f} f + \sum_{k=3}^{4} s^f_k H^0_k \bar{f} \gamma^5 f \tag{A7}$$

with the couplings

$$\begin{aligned}
&s^t_1 = -g \frac{m_t \cos\alpha}{2 m_W \sin\beta} = -\frac{h_t}{\sqrt{2}} \cos\alpha, \qquad s^b_1 = g \frac{m_b \sin\alpha}{2 m_W \cos\beta} = \frac{h_b}{\sqrt{2}} \sin\alpha, \qquad s^t_2 = -g \frac{m_t \sin\alpha}{2 m_W \sin\beta} = -\frac{h_t}{\sqrt{2}} \sin\alpha, \\
&s^b_2 = -g \frac{m_b \cos\alpha}{2 m_W \cos\beta} = -\frac{h_b}{\sqrt{2}} \cos\alpha, \qquad s^t_3 = ig \frac{m_t \cot\beta}{2 m_W} = i \frac{h_t}{\sqrt{2}} \cos\beta, \qquad s^b_3 = ig \frac{m_b \tan\beta}{2 m_W} = i \frac{h_b}{\sqrt{2}} \sin\beta, \\
&s^t_4 = ig \frac{m_t}{2 m_W} = i \frac{h_t}{\sqrt{2}} \sin\beta, \qquad s^b_4 = -ig \frac{m_b}{2 m_W} = -i \frac{h_b}{\sqrt{2}} \cos\beta.
\end{aligned} \tag{A8}$$

Here, h_t and h_b are the Yukawa couplings

$$h_t = \frac{g m_t}{\sqrt{2} m_W \sin\beta}, \qquad h_b = \frac{g m_b}{\sqrt{2} m_W \cos\beta}. \tag{A9}$$

The interaction Lagrangian for neutral Higgs bosons and neutralinos is given by

$$\mathcal{L} = -\frac{g}{2} \sum_{k=1}^{2} H^0_k \bar{\tilde{\chi}}^0_l F^0_{lmk} \tilde{\chi}^0_m - i \frac{g}{2} \sum_{k=3}^{4} H^0_k \bar{\tilde{\chi}}^0_l F^0_{lmk} \gamma_5 \tilde{\chi}^0_m$$

with

$$\begin{aligned}
F^0_{lmk} &= +\frac{e_k}{2} [Z_{l3} Z_{m2} + Z_{m3} Z_{l2} - \tan\theta_W (Z_{l3} Z_{m1} + Z_{m3} Z_{l1})] \\
&\quad + \frac{d_k}{2} [Z_{l4} Z_{m2} + Z_{m4} Z_{l2} - \tan\theta_W (Z_{l4} Z_{m1} + Z_{m4} Z_{l1})] \\
&= F^0_{mlk},
\end{aligned} \tag{A10}$$

where d_k and e_k take the values

$$\begin{aligned}
d_k &= \{-\cos\alpha, -\sin\alpha, \cos\beta, \sin\beta\}, \\
e_k &= \{-\sin\alpha, \cos\alpha, -\sin\beta, \cos\beta\}.
\end{aligned}$$

Following Ref. [40], the neutral Higgs-boson-sfermion-sfermion couplings can be written as

$$G^{\tilde{f}}_{ijk} \equiv G(H^0_k \tilde{f}^*_i \tilde{f}_j) = [R^{\tilde{f}} G^{\tilde{f}}_{LR,k} (R^{\tilde{f}})^T]_{ij}, \tag{A11}$$

where the left-right couplings $G^{\tilde{f}}_{LR,k}$ for third-generation up- and down-type sfermions are

$$G^{\tilde{t}}_{LR,1} = \begin{pmatrix} -\sqrt{2}h_t m_t c_\alpha + g_Z m_Z (I^{3L}_t - e_t s^2_W) s_{\alpha+\beta} & -\frac{h_t}{\sqrt{2}}(A_t c_\alpha + \mu s_\alpha) \\ -\frac{h_t}{\sqrt{2}}(A_t c_\alpha + \mu s_\alpha) & -\sqrt{2}h_t m_t c_\alpha + g_Z m_Z e_t s^2_W s_{\alpha+\beta} \end{pmatrix},$$

$$G^{\tilde{b}}_{LR,1} = \begin{pmatrix} \sqrt{2}h_b m_b s_\alpha + g_Z m_Z (I^{3L}_b - e_b s^2_W) s_{\alpha+\beta} & \frac{h_b}{\sqrt{2}}(A_b s_\alpha + \mu c_\alpha) \\ \frac{h_b}{\sqrt{2}}(A_b s_\alpha + \mu c_\alpha) & \sqrt{2}h_b m_b s_\alpha + g_Z m_Z e_b s^2_W s_{\alpha+\beta} \end{pmatrix},$$

$$G^{\tilde{f}}_{LR,2} = G^{\tilde{f}}_{LR,1} \quad \text{with } \alpha \to \alpha - \pi/2,$$

$$G^{\tilde{t}}_{LR,3} = -\sqrt{2}h_t \begin{pmatrix} 0 & -\frac{i}{2}(A_t c_\beta + \mu s_\beta) \\ \frac{i}{2}(A_t c_\beta + \mu s_\beta) & 0 \end{pmatrix},$$

$$G^{\tilde{b}}_{LR,3} = -\sqrt{2}h_b \begin{pmatrix} 0 & -\frac{i}{2}(A_b s_\beta + \mu c_\beta) \\ \frac{i}{2}(A_b s_\beta + \mu c_\beta) & 0 \end{pmatrix},$$

$$G^{\tilde{f}}_{LR,4} = G^{\tilde{f}}_{LR,3} \quad \text{with } \beta \to \beta - \pi/2.$$

Here, we have used the abbreviations $s_x \equiv \sin x$ and $c_x \equiv \cos x$ and α denotes the mixing angle of the $\{h^0, H^0\}$-system.

For the neutralino-sfermion-fermion couplings, the Lagrangian reads

$$\mathcal{L} = \bar{f}(a^{\tilde{f}}_{ik} P_R + b^{\tilde{f}}_{ik} P_L)\tilde{\chi}^0_k \tilde{f}_i + \bar{\tilde{\chi}}^0_k (a^{\tilde{f}}_{ik} P_L + b^{\tilde{f}}_{ik} P_R) f \tilde{f}^*_i \tag{A12}$$

with the coupling matrices

$$\begin{aligned} a^{\tilde{f}}_{ik} &= h_f Z_{kx} R^{\tilde{f}}_{i2} + g f^f_{Lk} R^{\tilde{f}}_{i1}, \\ b^{\tilde{f}}_{ik} &= h_f Z_{kx} R^{\tilde{f}}_{i1} + g f^f_{Rk} R^{\tilde{f}}_{i2} \end{aligned} \tag{A13}$$

and

$$\begin{aligned} f^f_{Lk} &= \sqrt{2}((e_f - I^{3L}_f)\tan\theta_W Z_{k1} + I^{3L}_f Z_{k2}), \\ f^f_{Rk} &= -\sqrt{2} e_f \tan\theta_W Z_{k1}. \end{aligned} \tag{A14}$$

The coupling of gluinos to sfermions and fermions can be derived from the Lagrangian

$$\begin{aligned} \mathcal{L} = -\sqrt{2} g_s T^a_{st} [&\bar{f}_s (R_{iL} P_R - R_{iR} P_L)\tilde{g}^a \tilde{f}_{i,t} \\ &+ \bar{\tilde{g}}^a (R_{iL} P_L - R_{iR} P_R) f_s \tilde{f}^*_{i,t}], \end{aligned} \tag{A15}$$

where $g_s = \sqrt{4\pi\alpha_s}$ is the strong coupling constant and R is the sfermion mixing matrix defined above. Finally, the Lagrangian corresponding to the couplings of the gluon to fermions and sfermions is

$$\mathcal{L} = -g_s T^a_{st} g^a_\mu \bar{f}_s \gamma^\mu f_t - i g_s T^a_{st} g^a_\mu \tilde{f}^*_{i,s} \overleftrightarrow{\partial^\mu} \tilde{f}_{j,t}, \tag{A16}$$

where the T^a represent the usual SU(3) color matrices.

APPENDIX B: VIRTUAL CORRECTIONS

Here, we give explicit forms of the next-to-leading order amplitudes $\mathcal{M}_{1\text{-loop}}$ mentioned in Sec. II. We use generic amplitudes with generic couplings, which we then specify using the couplings given in Appendix A. Note that all kinds of indices are to be summed over even if not explicitly stated. We leave out the results for self-energies, which can be found in [19] using the same conventions and couplings.

1. Vertex corrections

The contribution of the vertex corrections depicted in Fig. 2 to the matrix element $\mathcal{M}_{1\text{-loop}}$ can be written in terms of six loop diagrams. Denoting the momenta of the incoming neutralinos p_1 and p_2 and those of the outgoing quark and antiquark as k_1 and k_2, the next-to-leading corrections to the s-channel exchange of the Z^0-boson can be parametrized as

$$\begin{aligned} \mathcal{M}_{1\text{-loop}} = [\bar{v}(p_2)\gamma^\mu (A_L P_L + A_R P_R) u(p_1)] &\frac{-i g_{\mu\nu}}{s - m^2_Z} \\ &\times [\bar{u}(k_1)\{\gamma^\nu (B^1_L P_L + B^1_R P_R) \\ &+ k^\nu_1 (B^2_L P_L + B^2_R P_R) \\ &+ k^\nu_2 (B^3_L P_L + B^3_R P_R)\} v(k_2)] \end{aligned} \tag{B1}$$

where A_L, A_R are the chiral couplings of two neutralinos to the Z^0-boson

$$A_L = -A_R = -\frac{g}{2c_W}(Z_{i3} Z_{j3} + Z_{i4} Z_{j4}) \tag{B2}$$

and B^i_L, B^i_R are general form factors, which will now be given for the loops with a gluon and a gluino exchange. The form factors for the loop diagram containing a gluon (on the left side in Fig. 13) are

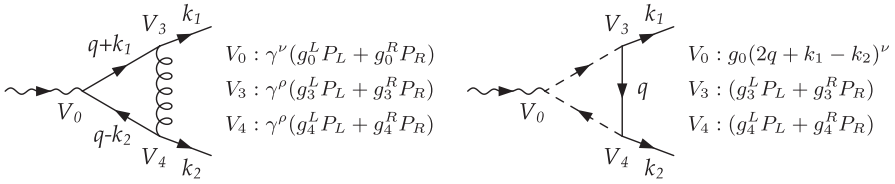

FIG. 13. Vertex corrections to the Z^0-boson coupling to quarks, where the arrows indicate the flow of the four-momenta and q is the independent loop-momentum.

$$B_L^1 = \frac{1}{8\pi^2} g_3^L g_4^L [g_0^L (B_0 - 2C_{00} - s(C_0 + C_1 + C_2) + m_f^2(2C_0 + 3C_1 + 3C_2)) + g_0^R m_f^2 (C_1 + C_2)], \tag{B3}$$

$$B_L^2 = -\frac{1}{4\pi^2} g_3^L g_4^L m_f [g_0^L C_{11} + g_0^R (C_{12} + C_2)], \tag{B4}$$

$$B_L^3 = \frac{1}{4\pi^2} g_3^L g_4^L m_f [g_0^L (C_1 + C_{12}) + g_0^R C_{22}], \tag{B5}$$

$$B_R^i = B_L^i (g_0^L \leftrightarrow g_0^R), \qquad i = 1, 2, 3. \tag{B6}$$

Using the notation from Appendix A, the generic couplings in this case are

$$\begin{aligned} g_0^L &= \frac{g}{c_W} C_L^f, \qquad g_0^R = \frac{g}{c_W} C_R^f, \\ g_3^L &= g_3^R = g_4^L = g_4^R = -g_s T_{st}^a. \end{aligned} \tag{B7}$$

The scalar loop integrals follow the definition given in Ref. [41] and their arguments are

$$C_i(k_1, -k_2; 0, m_f, m_f), \qquad B_0(-k_1 - k_2; m_f, m_f), \tag{B8}$$

where m_f is the mass of the final-state fermion.

The same form factors for the diagram with a gluino exchange (see Fig. 13 right) are given as

$$B_L^1 = \frac{1}{8\pi^2} g_0 g_3^R g_4^L C_{00}, \tag{B9}$$

$$B_L^2 = \frac{1}{16\pi^2} g_0 [g_4^L (-g_3^L m_{\tilde{g}} (C_0 + 2C_1) + g_3^R m_f (C_1 + 2C_{11})) - g_4^R g_3^L m_f (C_2 + 2C_{12})], \tag{B10}$$

$$B_L^3 = -\frac{1}{16\pi^2} g_0 [g_4^L (-g_3^L m_{\tilde{g}} (C_0 + 2C_2) + g_3^R m_f (C_1 + 2C_{12})) + g_4^R g_3^L m_f (C_2 + 2C_{22})], \tag{B11}$$

$$B_R^i = B_L^i (g_3^L \leftrightarrow g_3^R, g_4^L \leftrightarrow g_4^R), \qquad i = 1, 2, 3, \tag{B12}$$

where the couplings are

$$\begin{aligned} g_0 &= -\frac{g}{c_W} z_{ij}^{\tilde{f}}, \\ g_3^L &= \sqrt{2} g_s T_{st}^a R_{i2}, \qquad g_3^R = -\sqrt{2} g_s T_{st}^a R_{i1}, \\ g_4^L &= -\sqrt{2} g_s T_{st}^a R_{j1}, \qquad g_4^R = \sqrt{2} g_s T_{st}^a R_{j2}. \end{aligned} \tag{B13}$$

Here, the arguments of the loop integrals are

$$C_i(k_1, -k_2; m_{\tilde{g}}, m_{\tilde{f}_i}, m_{\tilde{f}_j}), \qquad B_0(-k_1 - k_2; m_{\tilde{f}_i}, m_{\tilde{f}_j}). \tag{B14}$$

The generic structure of the amplitude, which parametrizes the corrections to the s-channel Higgs-boson exchanges, is much simpler and can be written as

$$\mathcal{M}_{1\text{-loop}} = \sum_{k=1}^{4} [\bar{v}(p_2)(C_{L,k} P_L + C_{R,k} P_R) u(p_1)] \frac{i}{s - m_{H_k}^2} \times [\bar{u}(k_1)(D_{L,k}^1 P_L + D_{R,k}^1 P_R) v(k_2)], \tag{B15}$$

where $C_{L,k}$ and $C_{R,k}$ are the couplings of the two neutrali-

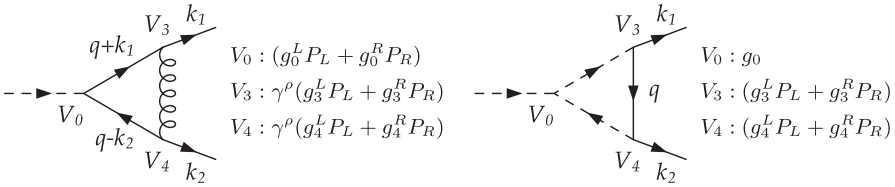

FIG. 14. Vertex corrections to the H_k^0-boson coupling to fermions, where the arrows indicate the flow of the four-momenta and q is the independent loop momentum.

nos to the Higgs boson

$$C_{L,k} = C_{R,k} = -\frac{g}{2} F^0_{11k} \quad \text{for } k = 1, 2, \tag{B16}$$

$$C_{L,k} = -C_{R,k} = \frac{g}{2} F^0_{11k} \quad \text{for } k = 3, 4. \tag{B17}$$

There are only two form factors D^1_L and D^1_R, which receive contributions from two diagrams (see Fig. 14). The contribution in the case of the gluon exchange is

$$D^1_L = \frac{1}{8\pi^2} g^L_3 g^L_4 [g^L_0 (2B_0 - m_f^2 C_0 + (-s + 3m_f^2) \times (C_0 + C_1 + C_2)) - g^R_0 m_f^2 (C_1 + C_2)], \tag{B18}$$

$$D^1_R = D^1_L (g^L_0 \leftrightarrow g^R_0), \tag{B19}$$

where the couplings are

$$\begin{aligned} &g^L_0 = g^R_0 = s^f_k \qquad (k = 1, 2), \\ &g^L_0 = -g^R_0 = -s^f_k \qquad k = (3, 4), \\ &g^L_3 = g^R_3 = g^L_4 = g^R_4 = -g_s T^a_{st}. \end{aligned} \tag{B20}$$

The loop integrals are identical to those defined in Eq. (B8).

The same form factors for the gluino contribution are

$$D^1_L = \frac{1}{16\pi^2} g_0 [-g^L_3 g^L_4 m_{\tilde{g}} C_0 + g^R_3 g^L_4 m_f C_1 + g^L_3 g^R_4 m_f C_2], \tag{B21}$$

$$D^1_R = D^1_L (g^L_3 \leftrightarrow g^R_3, g^L_4 \leftrightarrow g^R_4), \tag{B22}$$

where the couplings are

$$\begin{aligned} &g_0 = G^{\tilde{f}}_{ijk}, \qquad g^L_3 = \sqrt{2} g_s T^a_{st} R_{i2}, \qquad g^R_3 = -\sqrt{2} g_s T^a_{st} R_{i1}, \\ &g^L_4 = -\sqrt{2} g_s T^a_{st} R_{j1}, \qquad g^R_4 = \sqrt{2} g_s T^a_{st} R_{j2}, \end{aligned} \tag{B23}$$

and the loop integrals are defined in the same manner as in Eq. (B14).

The remaining vertex corrections are those connected with the t- and u-channel squark exchanges, where we have defined $t = (p_1 - k_2)^2$ and $u = (p_1 - k_1)^2$. We give here just the results for the t-channel, since the u-channel can obtained by using the crossing symmetry. The generic amplitude is

$$\begin{aligned} \mathcal{M}_{\text{1-loop}} = &\sum_{i=1}^{2} [\bar{u}(k_1)(E^1_{L,i} P_L + E^1_{R,i} P_R) u(p_2)] \frac{i}{t - m^2_{\tilde{f}_i}} \\ &\times [\bar{v}(p_1)(F_{L,i} P_L + F_{R,i} P_R) v(k_2)] \\ &+ \sum_{i=1}^{2} [\bar{u}(k_1)(E_{L,i} P_L + E_{R,i} P_R) u(p_2)] \\ &\times \frac{i}{t - m^2_{\tilde{f}_i}} [\bar{v}(p_1)(F^1_{L,i} P_L + F^1_{R,i} P_R) v(k_2)], \end{aligned} \tag{B24}$$

where $E_{L/R,i}$ and $F_{L/R,i}$ are tree-level couplings given as

$$\begin{aligned} &E_{L,i} = b^{\tilde{f}}_{i1}, \qquad E_{R,i} = a^{\tilde{f}}_{i1}, \\ &F_{L,i} = E_{R,i}, \qquad F_{R,i} = E_{L,i}. \end{aligned} \tag{B25}$$

The contribution of the gluon exchange diagram (see Fig. 15 left) is

$$E^1_L = \frac{1}{16\pi^2} g_0 g^L_3 [g^L_4 (B_0 + 2m_f^2 (C_0 - C_1) + (s + t) C_1 + m^2_{\tilde{\chi}} (C_2 - C_1)) - g^R_4 m_{\tilde{\chi}} m_f (C_0 + C_2 + C_1)], \tag{B26}$$

$$E^1_R = E^1_L (g^L_4 \leftrightarrow g^R_4), \tag{B27}$$

$$F^1_L = E^1_R, \tag{B28}$$

$$F^1_R = E^1_L, \tag{B29}$$

where the couplings are

$$\begin{aligned} &g_0 = -g_s T^a_{st} \delta_{ij}, \qquad g^L_3 = g^R_3 = -g_s T^a_{st} \\ &g^L_4 = b^{\tilde{f}}_{j1}, \qquad g^R_4 = a^{\tilde{f}}_{j1} \end{aligned} \tag{B30}$$

and the scalar loop coefficients have the arguments

$$C_i(-k_1, -p_2; m_f, 0, m_{\tilde{f}_j}), \qquad B_0(k_1 - p_2; 0, m_{\tilde{f}_j}). \tag{B31}$$

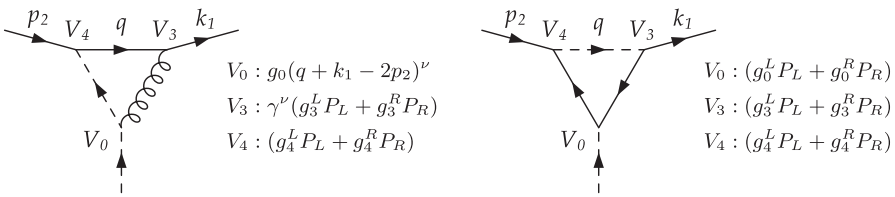

FIG. 15. Vertex corrections to the neutralino coupling to a fermion and a sfermion where the arrows indicate the flow of the four-momenta and q is the independent loop momentum.

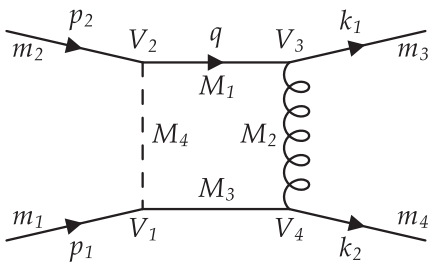

$V_1: \; a^{\tilde{q}}_{ij} P_L + b^{\tilde{q}}_{ij} P_R$

$V_2: \; b^{\tilde{q}}_{ik} P_L + a^{\tilde{q}}_{ik} P_R$

$V_3: \; -g_s T^a_{st} \gamma^\mu$

$V_4: \; -g_s T^a_{ts} \gamma^\mu$

FIG. 16. Conventions and notations used for momenta, masses, and couplings in the calculation of the box diagram arising from the exchange of a gluon between the two final-state quarks in neutralino-pair annihilation. The arrows indicate the direction of defined four-momenta. The coupling strengths are defined in Appendix A.

The gluino contribution gives

$$\begin{aligned} E^1_L = -\frac{1}{16\pi^2}[&g^L_0 g^L_3 g^L_4 m_{\tilde{g}} m_f C_0 + g^L_0 g^L_3 g^R_4 m_{\tilde{g}} m_{\tilde{\chi}} (C_0 + C_2) \\ &+ g^L_0 g^R_3 g^L_4 m^2_f (C_0 + C_1) + g^R_0 g^R_3 g^L_4 m_{\tilde{g}} m_f C_1 \\ &+ g^L_0 g^R_3 g^R_4 m_{\tilde{\chi}} m_f (C_0 + C_1 + C_2) \\ &+ g^R_0 g^L_3 g^L_4 (B_0 + m^2_{\tilde{f}_j} C_0 + m^2_f C_1 + m^2_{\tilde{\chi}} C_2) \\ &+ g^R_0 g^L_3 g^R_4 m_f m_{\tilde{\chi}} C_2], \end{aligned} \tag{B32}$$

$$E^1_R = E^1_L (g^L_0 \leftrightarrow g^R_0, g^L_3 \leftrightarrow g^R_3, g^L_4 \leftrightarrow g^R_4), \tag{B33}$$

$$F^1_L = E^1_R, \tag{B34}$$

$$F^1_R = E^1_L, \tag{B35}$$

where the couplings are given by

$$\begin{aligned} &g^L_0 = \sqrt{2} g_s T^a_{st} R_{i2}, \quad g^L_3 = \sqrt{2} g_s T^a_{st} R_{j2}, \quad g^L_4 = a^{\tilde{f}}_{j1}, \\ &g^R_0 = -\sqrt{2} g_s T^a_{st} R_{i1}, \quad g^R_3 = -\sqrt{2} g_s T^a_{st} R_{j1}, \quad g^R_4 = b^{\tilde{f}}_{j1}, \end{aligned} \tag{B36}$$

and the scalar loop functions are

$$C_i(-k_1, -p_2; m_{\tilde{f}_j}, m_{\tilde{g}}, m_f), \qquad B_0(k_1 - p_2; m_{\tilde{g}}, m_f). \tag{B37}$$

2. Box corrections

At the one-loop level, the neutralino annihilation into quark-antiquark pairs receives box contributions arising from the exchange of a gluon or a gluino between the final-state quarks (see Fig. 2). In order to express the corresponding amplitudes in a rather generic way, we introduce the notations shown in Figs. 16 and 17 for the gluon and gluino box, respectively. The momenta of the incoming neutralinos are again labeled p_1 and p_2, those of the outgoing quarks are k_1 and k_2. The corresponding external masses are m_i $(i = 1, \ldots, 4)$, while the masses of the internal particles are denoted M_i $(i = 1, \ldots, 4)$. The left- and right-handed coupling strengths, which correspond to the vertices appearing in the schematic diagram, are generically denoted by $g^{L,R}_i$ $(i = 1, \ldots, 4)$. For the sake of compact expressions, we use in the following the abbreviations

$$\mathcal{V}_i = g^L_i P_L + g^R_i P_R, \qquad \overline{\mathcal{V}}_i = g^L_i P_R + g^R_i P_L, \tag{B38}$$

where P_L and P_R are the left- and right-handed chirality projectors, respectively. The independent loop-momentum q is defined to be the momentum of the particle having the mass M_1 as shown in Figs. 16 and 17. The arising tensor integrals have been reduced to scalar integrals

$$D_{\{i,ij\}} \equiv D_{\{i,ij\}}(-k_1, -(p_1 + p_2), -p_2; M_1, M_2, M_3, M_4) \tag{B39}$$

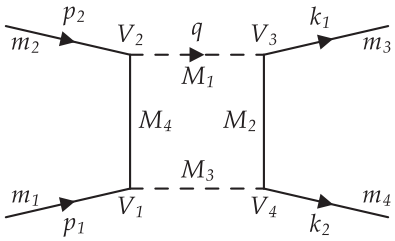

$V_1: \; b^{\tilde{q}}_{ik} P_L + a^{\tilde{q}}_{ik} P_R$

$V_2: \; a^{\tilde{q}}_{jk} P_L + b^{\tilde{q}}_{jk} P_R$

$V_3: \; -\sqrt{2} g_s T^a_{st} \left(R_{jL} P_L - R_{jR} P_R \right)$

$V_4: \; -\sqrt{2} g_s T^a_{st} \left(R_{iR} P_L - R_{iL} P_R \right)$

FIG. 17. Same as Fig. 16 for the exchange of a gluino between the two final-state quarks.

for $i, j = 0, \ldots, 3$. For their definition and the applied convention we refer the reader to Ref. [41].

In case of the gluon box, the amplitude can be written as

$$i\mathcal{M}^{(g)}_{\text{box}} = -\bar{u}(k_1)\mathcal{F}^1_0 u(p_2)\bar{v}(p_1)\mathcal{F}^2_0 v(k_2)D_0 - \sum_{i=1}^{3}\sum_{k=1}^{2}\bar{u}(k_1)\mathcal{F}^{2k-1}_i u(p_2)\bar{v}(p_1)\mathcal{F}^{2k}_i v(k_2)D_i - \bar{u}(k_1)\mathcal{F}^1_{00}u(p_2)\bar{v}(p_1)\mathcal{F}^2_{00}v(k_2)D_{00} - \sum_{i,j=1}^{3}\bar{u}(k_1)\mathcal{F}^1_{ij}u(p_2)\bar{v}(p_1)\mathcal{F}^2_{ij}v(k_2)D_{ij}, \tag{B40}$$

where the form factors are given by

$$\begin{aligned}
&\mathcal{F}^1_0 = m_1\gamma^\mu\mathcal{V}_3\mathcal{V}_2, \quad \mathcal{F}^2_0 = m_3\mathcal{V}_1\gamma_\mu\mathcal{V}_4 + M_1\overline{\mathcal{V}}_1\gamma_\mu\mathcal{V}_4 - \not{p}_2\overline{\mathcal{V}}_1\gamma_\mu\mathcal{V}_4, \quad \mathcal{F}^1_1 = M_3\gamma^\mu\overline{\mathcal{V}}_3\mathcal{V}_2 - 2k_1^\mu\overline{\mathcal{V}}_3\mathcal{V}_2,\\
&\mathcal{F}^2_1 = m_3\mathcal{V}_1\gamma_\mu\mathcal{V}_4 + M_1\overline{\mathcal{V}}_1\gamma_\mu\mathcal{V}_4 - \not{p}_2\overline{\mathcal{V}}_1\gamma_\mu\mathcal{V}_4, \quad \mathcal{F}^3_1 = -m_1\gamma^\mu\mathcal{V}_3\mathcal{V}_2, \quad \mathcal{F}^4_1 = \not{k}_1\overline{\mathcal{V}}_1\gamma_\mu\mathcal{V}_4,\\
&\mathcal{F}^1_2 = -\gamma^\mu\not{p}_1\overline{\mathcal{V}}_3\mathcal{V}_2 - M_2\gamma^\mu\mathcal{V}_3\overline{\mathcal{V}}_2, \quad \mathcal{F}^2_2 = m_3\mathcal{V}_1\gamma_\mu\mathcal{V}_4 + M_1\overline{\mathcal{V}}_1\gamma_\mu\mathcal{V}_4 - \not{p}_2\overline{\mathcal{V}}_1\gamma_\mu\mathcal{V}_4,\\
&\mathcal{F}^3_2 = m_1\gamma^\mu\mathcal{V}_3\mathcal{V}_2, \quad \mathcal{F}^4_2 = M_1\overline{\mathcal{V}}_1\gamma_\mu\mathcal{V}_4 - \not{p}_2\overline{\mathcal{V}}_1\gamma_\mu\mathcal{V}_4, \quad \mathcal{F}^1_3 = -M_2\gamma^\mu\mathcal{V}_3\overline{\mathcal{V}}_2,\\
&\mathcal{F}^2_3 = m_3\mathcal{V}_1\gamma_\mu\mathcal{V}_4 + M_1\overline{\mathcal{V}}_1\gamma_\mu\mathcal{V}_4 - \not{p}_2\overline{\mathcal{V}}_1\gamma_\mu\mathcal{V}_4, \quad \mathcal{F}^3_3 = m_1\gamma^\mu\mathcal{V}_3\mathcal{V}_2, \quad \mathcal{F}^4_3 = \not{p}_2\overline{\mathcal{V}}_1\gamma_\mu\mathcal{V}_4,\\
&\mathcal{F}^1_{00} = \gamma^\mu\mathcal{V}_3\gamma^\nu\mathcal{V}_2, \quad \mathcal{F}^2_{00} = \mathcal{V}_1\gamma_\nu\gamma_\mu\mathcal{V}_4, \quad \mathcal{F}^1_{11} = 2k_1^\mu\overline{\mathcal{V}}_3\mathcal{V}_2 - M_3\gamma^\mu\overline{\mathcal{V}}_3\mathcal{V}_2, \quad \mathcal{F}^2_{11} = \not{k}_1\overline{\mathcal{V}}_1\gamma_\mu\mathcal{V}_4,\\
&\mathcal{F}^1_{12} = 2k_1^\mu\overline{\mathcal{V}}_3\mathcal{V}_2 - M_3\gamma^\mu\overline{\mathcal{V}}_3\mathcal{V}_2, \quad \mathcal{F}^2_{12} = -M_1\overline{\mathcal{V}}_1\gamma_\mu\mathcal{V}_4 + \not{p}_2\overline{\mathcal{V}}_1\gamma_\mu\mathcal{V}_4,\\
&\mathcal{F}^1_{13} = 2k_1^\mu\overline{\mathcal{V}}_3\mathcal{V}_2 - M_3\gamma^\mu\overline{\mathcal{V}}_3\mathcal{V}_2, \quad \mathcal{F}^2_{13} = \not{p}_2\overline{\mathcal{V}}_1\gamma_\mu\mathcal{V}_4
\end{aligned} \tag{B41}$$

$$\begin{aligned}
&\mathcal{F}^1_{21} = \gamma^\mu\not{p}_1\overline{\mathcal{V}}_3\mathcal{V}_2 + M_2\gamma^\mu\mathcal{V}_3\overline{\mathcal{V}}_2, \quad \mathcal{F}^2_{21} = \not{k}_1\overline{\mathcal{V}}_1\gamma_\mu\mathcal{V}_4, \quad \mathcal{F}^1_{22} = \gamma^\mu\not{p}_1\overline{\mathcal{V}}_3\mathcal{V}_2 + M_2\gamma^\mu\mathcal{V}_3\overline{\mathcal{V}}_2,\\
&\mathcal{F}^2_{22} = -M_1\overline{\mathcal{V}}_1\gamma_\mu\mathcal{V}_4 + \not{p}_2\overline{\mathcal{V}}_1\gamma_\mu\mathcal{V}_4, \quad \mathcal{F}^1_{23} = \gamma^\mu\not{p}_1\overline{\mathcal{V}}_3\mathcal{V}_2 + M_2\gamma^\mu\mathcal{V}_3\overline{\mathcal{V}}_2, \quad \mathcal{F}^2_{23} = \not{p}_2\overline{\mathcal{V}}_1\gamma_\mu\mathcal{V}_4,\\
&\mathcal{F}^1_{31} = M_2\gamma^\mu\mathcal{V}_3\overline{\mathcal{V}}_2, \quad \mathcal{F}^2_{31} = \not{k}_1\overline{\mathcal{V}}_1\gamma_\mu\mathcal{V}_4, \quad \mathcal{F}^1_{32} = M_2\gamma^\mu\mathcal{V}_3\overline{\mathcal{V}}_2, \quad \mathcal{F}^2_{32} = -M_1\overline{\mathcal{V}}_1\gamma_\mu\mathcal{V}_4 + \not{p}_2\overline{\mathcal{V}}_1\gamma_\mu\mathcal{V}_4,\\
&\mathcal{F}^1_{33} = M_2\gamma^\mu\mathcal{V}_3\overline{\mathcal{V}}_2, \quad \mathcal{F}^2_{33} = \not{p}_2\overline{\mathcal{V}}_1\gamma_\mu\mathcal{V}_4.
\end{aligned} \tag{B42}$$

Using the same notation, the amplitude of the gluino box is given by

$$i\mathcal{M}^{(\tilde{g})}_{\text{box}} = \bar{v}(p_2)\mathcal{F}^1_0 u(p_1)\bar{u}(k_1)\mathcal{F}^2_0 v(k_2)D_0 + \sum_{i=1}^{3}\sum_{k=1}^{2}\bar{v}(p_2)\mathcal{F}^{2k-1}_i u(p_1)\bar{u}(k_1)\mathcal{F}^{2k}_i v(k_2)D_i + \bar{v}(p_2)\mathcal{F}^1_{00}u(p_1)\bar{u}(k_1)\mathcal{F}^2_{00}v(k_2)D_{00} + \sum_{i,j=1}^{3}\bar{v}(p_2)\mathcal{F}^1_{ij}u(p_1)\bar{u}(k_1)\mathcal{F}^2_{ij}v(k_2)D_{ij} \tag{B43}$$

with the form factors

$$\mathcal{F}_0^1 = m_4 \mathcal{V}_2 \mathcal{V}_1 + M_2 \overline{\mathcal{V}}_2 \mathcal{V}_1, \qquad \mathcal{F}_0^2 = m_2 \mathcal{V}_3 \mathcal{V}_4 + M_3 \overline{\mathcal{V}}_3 \mathcal{V}_4, \qquad \mathcal{F}_1^1 = \mathcal{V}_2 \not{k}_1 \mathcal{V}_1,$$
$$\mathcal{F}_1^2 = M_3 \overline{\mathcal{V}}_3 \mathcal{V}_4 + m_2 \mathcal{V}_3 \mathcal{V}_4, \qquad \mathcal{F}_1^3 = M_2 \overline{\mathcal{V}}_2 \mathcal{V}_1 + m_4 \mathcal{V}_2 \mathcal{V}_1, \qquad \mathcal{F}_1^4 = M_3 \overline{\mathcal{V}}_3 \mathcal{V}_4,$$
$$\mathcal{F}_2^1 = M_2 \overline{\mathcal{V}}_2 \mathcal{V}_1 - M_1 \mathcal{V}_2 \overline{\mathcal{V}}_1, \qquad \mathcal{F}_2^2 = M_3 \overline{\mathcal{V}}_3 \mathcal{V}_4 + m_2 \mathcal{V}_3 \mathcal{V}_4, \qquad \mathcal{F}_2^3 = M_2 \overline{\mathcal{V}}_2 \mathcal{V}_1 + m_4 \mathcal{V}_2 \mathcal{V}_1,$$
$$\mathcal{F}_2^4 = M_3 \overline{\mathcal{V}}_3 \mathcal{V}_4 - M_4 \mathcal{V}_3 \overline{\mathcal{V}}_4, \qquad \mathcal{F}_3^1 = M_2 \overline{\mathcal{V}}_2 \mathcal{V}_1, \qquad \mathcal{F}_3^2 = M_3 \overline{\mathcal{V}}_3 \mathcal{V}_4 + m_2 \mathcal{V}_3 \mathcal{V}_4,$$
$$\mathcal{F}_3^3 = M_2 \overline{\mathcal{V}}_2 \mathcal{V}_1 + m_4 \mathcal{V}_2 \mathcal{V}_1, \qquad \mathcal{F}_3^4 = -\mathcal{V}_3 \not{p}_2 \mathcal{V}_4, \qquad \mathcal{F}_{00}^1 = -\mathcal{V}_2 \gamma^\mu \mathcal{V}_1,$$
$$\mathcal{F}_{00}^2 = \mathcal{V}_3 \gamma_\mu \mathcal{V}_4, \qquad \mathcal{F}_{11}^1 = -\mathcal{V}_2 \not{k}_1 \mathcal{V}_1, \qquad \mathcal{F}_{11}^2 = M_3 \overline{\mathcal{V}}_3 \mathcal{V}_4, \qquad \mathcal{F}_{12}^1 = -\mathcal{V}_2 \not{k}_1 \mathcal{V}_1,$$
$$\mathcal{F}_{12}^2 = M_3 \overline{\mathcal{V}}_3 \mathcal{V}_4 - M_4 \mathcal{V}_3 \overline{\mathcal{V}}_4, \qquad \mathcal{F}_{13}^1 = -\mathcal{V}_2 \not{k}_1 \mathcal{V}_1, \qquad \mathcal{F}_{13}^2 = \mathcal{V}_3 \not{p}_2 \mathcal{V}_4, \qquad \mathcal{F}_{21}^1 = M_2 \overline{\mathcal{V}}_2 \mathcal{V}_1 - M_1 \mathcal{V}_2 \overline{\mathcal{V}}_1,$$
$$\mathcal{F}_{21}^2 = M_3 \overline{\mathcal{V}}_3 \mathcal{V}_4, \qquad \mathcal{F}_{22}^1 = M_2 \overline{\mathcal{V}}_2 \mathcal{V}_1 - M_1 \mathcal{V}_2 \overline{\mathcal{V}}_1, \qquad \mathcal{F}_{22}^2 = M_3 \overline{\mathcal{V}}_3 \mathcal{V}_4 - M_4 \mathcal{V}_3 \overline{\mathcal{V}}_4,$$
$$\mathcal{F}_{23}^1 = M_2 \overline{\mathcal{V}}_2 \mathcal{V}_1 - M_1 \mathcal{V}_2 \overline{\mathcal{V}}_1, \qquad \mathcal{F}_{23}^2 = \mathcal{V}_3 \not{p}_2 \mathcal{V}_4, \qquad \mathcal{F}_{31}^1 = M_2 \overline{\mathcal{V}}_2 \mathcal{V}_1, \qquad \mathcal{F}_{31}^2 = M_3 \overline{\mathcal{V}}_3 \mathcal{V}_4,$$
$$\mathcal{F}_{32}^1 = M_2 \overline{\mathcal{V}}_2 \mathcal{V}_1, \qquad \mathcal{F}_{32}^2 = M_3 \overline{\mathcal{V}}_3 \mathcal{V}_4 - M_4 \mathcal{V}_3 \mathcal{V}_4, \qquad \mathcal{F}_{33}^1 = M_2 \overline{\mathcal{V}}_2 \mathcal{V}_1, \qquad \mathcal{F}_{33}^2 = \mathcal{V}_3 \not{p}_2 \mathcal{V}_4. \tag{B44}$$

[1] G. Hinshaw *et al.* (WMAP Collaboration), Astrophys. J. Suppl. Ser. **180**, 225 (2009).
[2] P. Gondolo and G. Gelmini, Nucl. Phys. **B360**, 145 (1991).
[3] A. Arbey and F. Mahmoudi, arXiv:0906.0368.
[4] G. Bélanger, S. Kraml, and A. Pukhov, Phys. Rev. D **72**, 015003 (2005).
[5] N. Baro, F. Boudjema, and A. Semenov, Phys. Lett. B **660**, 550 (2008).
[6] M. Drees and M. M. Nojiri, Phys. Rev. D **47**, 376 (1993).
[7] G. Jungman, M. Kamionkowski, and K. Griest, Phys. Rep. **267**, 195 (1996).
[8] B. Herrmann and M. Klasen, Phys. Rev. D **76**, 117704 (2007).
[9] B. Herrmann, M. Klasen, and K. Kovařík, Phys. Rev. D **79**, 061701(R) (2009).
[10] G. Bélanger, F. Boudjema, A. Pukhov, and A. Semenov, Comput. Phys. Commun. **149**, 103 (2002); **174**, 577 (2006); **176**, 367 (2007); **180**, 747 (2009).
[11] K. Kovařík, C. Weber, H. Eberl, and W. Majerotto, Phys. Rev. D **72**, 053010 (2005).
[12] Tevatron Electroweak Working Group, CDF, and D0 Collaborations, arXiv:0808.1089.
[13] K. Melnikov and A. Yelkhovsky, Phys. Rev. D **59**, 114009 (1999); A. H. Hoang, Phys. Rev. D **61**, 034005 (1999); M. Beneke and A. Signer, Phys. Lett. B **471**, 233 (1999); A. A. Penin and A. A. Pivovarov, Nucl. Phys. **B549**, 217 (1999).
[14] H. Baer, J. Ferrandis, K. Melnikov, and X. Tata, Phys. Rev. D **66**, 074007 (2002).
[15] M. S. Carena, D. Garcia, U. Nierste, and C. E. M. Wagner, Nucl. Phys. **B577**, 88 (2000).
[16] J. Guasch, P. Häfliger, and M. Spira, Phys. Rev. D **68**, 115001 (2003).
[17] S. Catani, S. Dittmaier, M. H. Seymour, and Z. Trocsanyi, Nucl. Phys. **B627**, 189 (2002).
[18] J. Küblbeck, M. Böhm, and A. Denner, Comput. Phys. Commun. **60**, 165 (1990); T. Hahn and M. Perez-Victoria, Comput. Phys. Commun. **118**, 153 (1999); T. Hahn, Comput. Phys. Commun. **140**, 418 (2001); T. Hahn and C. Schappacher, Comput. Phys. Commun. **143**, 54 (2002).
[19] H. Eberl, Ph.D. thesis (in German), Vienna University of Technology, 1998; K. Kovařík, Ph.D. thesis, Comenius University, 2005.
[20] R. K. Ellis and G. Zanderighi, J. High Energy Phys. 02 (2008) 002.
[21] D. G. Cassel, L. Trindle Gennari, and R. H. Siemann, in *Proceedings of 1996 DPF/DPB Summer Study on New Directions for High-Energy Physics, Snowmass, Colorado* (Stanford Linear Accelerator Center, Stanford, 1997).
[22] G. Anderson, H. Baer, C. H. Chen, and X. Tata, Phys. Rev. D **61**, 095005 (2000).
[23] M. Olechowski and S. Pokorski, Phys. Lett. B **344**, 201 (1995).
[24] M. Ratz, arXiv:0711.1582.
[25] H. P. Nilles, S. Ramos-Sanchez, M. Ratz, and P. K. S. Vaudrevange, Eur. Phys. J. C **59**, 249 (2009).
[26] H. Baer, A. Mustafayev, S. Profumo, A. Belyaev, and X. Tata, J. High Energy Phys. 07 (2005) 065.
[27] J. R. Ellis, K. A. Olive, and Y. Santoso, Phys. Lett. B **539**, 107 (2002).
[28] J. R. Ellis, T. Falk, K. A. Olive, and Y. Santoso, Nucl. Phys. **B652**, 259 (2003).
[29] J. R. Ellis, A. Ferstl, K. A. Olive, and Y. Santoso, Phys. Rev. D **67**, 123502 (2003).
[30] J. R. Ellis, K. Enqvist, D. V. Nanopoulos, and K. Tamvakis, Phys. Lett. B **155**, 381 (1985).
[31] V. Bertin, E. Nezri, and J. Orloff, J. High Energy Phys. 02 (2003) 046.
[32] S. P. Martin, Phys. Rev. D **75**, 115005 (2007).

[33] H. Baer, A. Box, E. K. Park, and X. Tata, J. High Energy Phys. 08 (2007) 060.
[34] W. Porod, Comput. Phys. Commun. **153**, 275 (2003).
[35] C. Amsler *et al.* (Particle Data Group), Phys. Lett. B **667**, 1 (2008).
[36] T. Moroi, Phys. Rev. D **53**, 6565 (1996); **56**, 4424(E) (1997).
[37] E. Barberio *et al.* (Heavy Flavor Averaging Group (HFAG) Collaboration), arXiv:0704.3575.
[38] S. Heinemeyer, W. Hollik, and G. Weiglein, Comput. Phys. Commun. **124**, 76 (2000); Eur. Phys. J. C **9**, 343 (1999).
[39] G. Degrassi, P. Gambino, and P. Slavich, Comput. Phys. Commun. **179**, 759 (2008); Phys. Lett. B **635**, 335 (2006).
[40] J. F. Gunion, H. E. Haber, G. L. Kane, and S. Dawson, *The Higgs Hunter's Guide* (Addison-Wesley, Reading, MA, 1990); J. F. Gunion and H. E. Haber, Nucl. Phys. **B272**, 1 (1986); **B402**, 567(E) (1993).
[41] A. Denner, Fortschr. Phys. **41**, 307 (1993).